

001  
002  
003  
004  
005  
006  
007  
008  
009  
010  
011  
012  
013  
014  
015  
016  
017  
018  
019  
020  
021  
022  
023  
024  
025  
026  
027  
028  
029  
030  
031  
032  
033  
034  
035  
036  
037  
038  
039  
040  
041  
042  
043  
044  
045  
046

# Microbial symbionts buffer hosts from the demographic costs of environmental stochasticity

Joshua C. Fowler<sup>1,2\*</sup>, Shaun Ziegler<sup>3</sup>, Kenneth D. Whitney<sup>3</sup>,  
Jennifer A. Rudgers<sup>3</sup>, Tom E.X. Miller<sup>1</sup>

<sup>1</sup>\*Department of BioSciences, Rice University, Houston, 77005, TX, USA.

<sup>2</sup>Department of Biology, University of Miami, Miami, 33146, FL, USA.

<sup>3</sup>Department of Biology, University of New Mexico, Albuquerque, 87131, NM, USA.

\*Corresponding author(s). E-mail(s): [jcf221@miami.edu](mailto:jcf221@miami.edu);

Contributing authors: [shaun.ziegler@gmail.com](mailto:shaun.ziegler@gmail.com); [whitneyk@unm.edu](mailto:whitneyk@unm.edu);

[jrudgers@unm.edu](mailto:jrudgers@unm.edu); [tom.miller@rice.edu](mailto:tom.miller@rice.edu);

Phone: 719-359-2960

#### Author Contributions

J.C.F. contributed to data collection, data analysis, and led manuscript drafting. S.Z. contributed to data collection and manuscript revisions. K.D.W. contributed to research conception, data collection, and manuscript revisions. J.A.R. established transplant plots, contributed to research conception, data collection, and manuscript revisions. T.E.X.M. contributed to research conception, data collection, data analysis, and manuscript revisions.

#### Data and Code Accessibility

Data will be made accessible as an Environmental Data Initiative package online  
**DOI:** [updated here when available](#). Code for all analysis is available through  
<https://github.com/joshuacfowler/Grass-Endophyte-Stochastic-Demography>

**Article Type:** Letter

**Running Title:** Symbiont-mediated demographic buffering

**Keywords:** stochasticity, demography, symbiosis, mutualism, Epichloë, Testing the differences

**This file contains:** Abstract ( 150 words), Main Text (5397 words), Figures (1-4); Supporting Information - Supplemental Methods, Supplemental Figures A1-A28, Supplemental Tables S1-S3, References (66)

047      Manuscript submitted following PNAS style guidelines and can be  
048                          reformatted upon revision  
049  
050  
051  
052  
053  
054  
055  
056  
057  
058  
059  
060  
061  
062  
063  
064  
065  
066  
067  
068  
069  
070  
071  
072  
073  
074  
075  
076  
077  
078  
079  
080  
081  
082  
083  
084  
085  
086  
087  
088  
089  
090  
091  
092

**Abstract**

Species' persistence in increasingly variable climates will depend on resilience against the fitness costs of environmental stochasticity. Most organisms host microbiota that shield against stressors. Here, we test the hypothesis that, by limiting exposure to environmental extremes, microbial symbionts reduce hosts' demographic variance. We parameterized stochastic models using data from a 14-year symbiont-removal experiment including seven grass species that host *Epichloë* fungal endophytes. Endophytes reduced variance in fitness by > 10%, on average. Hosts with "fast" life history traits that lacked longevity as an intrinsic buffer benefited most from symbiont-mediated variance buffering. Under current climate conditions, contributions of variance buffering were modest compared to symbiont benefits to mean fitness. However, simulations of increased stochasticity amplified benefits of variance buffering and made it the more important pathway of host-symbiont mutualism than elevated mean fitness. Microbial-mediated variance buffering is likely an important, yet cryptic, mechanism of resilience in an increasingly variable world.

093	
094	
095	
096	
097	
098	
099	
100	
101	
102	
103	
104	
105	
106	
107	
108	
109	
110	
111	
112	
113	
114	
115	
116	
117	
118	
119	
120	
121	
122	
123	
124	
125	
126	
127	
128	
129	
130	
131	
132	
133	
134	
135	
136	
137	
138	

139 **Introduction**

140  
141 **TESTING THE differences** Global climate change involves increases in environmental  
142 variability, including changes to precipitation patterns and the frequency of extreme  
143 weather events [1, 2]. Yet, the ecological consequences of increased variability are less  
144 well understood than those of changing climate means, such as long-term warming or  
145 drying. Incorporating environmental variability into forecasts of population dynamics  
146 can improve predictions of the future.

147 Classic theory predicts that long-term population growth rates (equivalently, pop-  
148 ulation mean fitness) will decline under increased environmental stochasticity because  
149 the costs of bad years outweigh the benefits of good years – a consequence of nonlinear  
150 averaging [3, 4]. For example, in unstructured populations, the long-term stochastic  
151 growth rate in a fluctuating environment ( $\lambda_s$ ) will always be lower than the average  
152 growth rate ( $\bar{\lambda}$ ) by an amount proportional to the environmental variance ( $\sigma^2$ ):

153  
154 
$$\log(\lambda_s) \approx \log(\bar{\lambda}) - \frac{\sigma^2}{2\bar{\lambda}^2} \quad (1)$$
  
155

156  
157 Populations structured by size or stage similarly experience costs of variability [5, 6].  
158 There are accordingly two pathways to increase population viability in a variable  
159 environment: increase the mean growth rate and/or dampen temporal fluctuation in  
160 growth rates, also called “variance buffering”.

161 Both the characteristics of species and the properties of their environment can  
162 buffer demographic fluctuations, including life history traits such as longevity [7, 8],  
163 correlations among vital rates [9], transient shifts in population structure [10], the  
164 magnitude of environmental variability [11], or the degree of environmental autocor-  
165 relation [12, 13]. These factors determine the risks of extinction faced by populations  
166 [14] and underlie management strategies promoting ecosystem resilience [15]. Yet little  
167 is known about how biotic interactions influence demographic variability or contribute  
168 to variance buffering [16].

169 Most multicellular organisms host symbiotic microbes that affect growth and per-  
170 formance [17, 18], and many of these are vertically transmitted from maternal hosts to  
171 offspring [19]. Vertical transmission links the fitness of hosts and symbionts in a feed-  
172 back loop that selects for mutual benefits [20]. Many vertically-transmitted microbes  
173 are mutualistic and protect hosts from stressful environmental conditions including  
174 drought, extreme temperatures, or natural enemies [21, 22]. Some of the best studied  
175 examples include bacterial symbionts of insects that provide their hosts with thermal  
176 tolerance through the production of heat-shock proteins [23], and fungal symbionts of  
177 plants that produce anti-herbivore and drought-protective compounds [24–26]. How-  
178 ever, these diverse protective symbioses are context-dependent: the magnitude of  
179 benefits depends on environmental conditions [27] and thus will vary temporally in  
180 a stochastic environment [28]. We hypothesized that context-dependent benefits from  
181 symbionts may buffer hosts against variability through strong benefits during harsh  
182 periods and neutral or even costly outcomes during benign periods, reducing the  
183 impacts of host exposure to extremes and dampening inter-annual variance relative  
184 to non-symbiotic hosts. Variance buffering is a previously unexplored mechanism by

which symbionts may benefit their hosts instead of or in addition to elevating average fitness, the focus of most previous research.	185
	186
We used a combination of long-term field experiments and stochastic demographic modeling to test the hypothesis that context-dependent benefits of symbiosis buffer hosts from the fitness costs of environmental stochasticity. We used cool-season grasses and <i>Epichloë</i> fungal endophytes as a tractable experimental model in which non-symbiotic plants can be derived from naturally symbiotic plants through heat treatment, providing a contrast of symbiont effects that controls for the confounding influence of host genetic background. <i>Epichloë</i> endophytes are specialized symbionts growing intercellularly in the aboveground tissue of ~ 30% of <i>C<sub>3</sub></i> grass species [29]. These fungi are primarily transmitted vertically from maternal plants through seeds [30]. They produce a variety of alkaloids that can protect host plants from natural enemies [31] and drought stress [32].	187
	188
	189
	190
	191
	192
	193
	194
	195
	196
	197
Over 14 years (2007–2021), we collected longitudinal demographic data on the survival, growth, reproduction, and recruitment of all plants within replicated endophyte-symbiotic and endophyte-free populations at our field site in southern Indiana, USA. Through taxonomic replication (seven host-symbiont species pairs) we aimed to understand whether host life history traits could explain inter-specific variation in the magnitude of demographic buffering through symbiosis. We used this long-term data to parameterize stochastic population projection models in a hierarchical Bayesian framework. Specifically, we (1) quantified the effect of symbiosis on the mean and variance of host vital rates (survival, growth and reproduction) and fitness, (2) evaluated the relationship between host life history traits and the magnitude of symbiont-mediated variance buffering, (3) determined the relative contribution of symbiont-mediated mean and variance effects to host fitness, and (4) projected how increased environmental stochasticity (expected under future climates) changes the importance of variance buffering as a pathway of host-symbiont mutualism.	198
	199
	200
	201
	202
	203
	204
	205
	206
	207
	208
	209
	210
	211
	212
<b>Materials and Methods</b>	213
<b>Study site and species</b>	214
This study was conducted at Indiana University's Lilly-Dickey Woods Research and Teaching Preserve (39.238533, -86.218150) in Brown County, Indiana, USA. This site is part of the Eastern broadleaf forests of southern Indiana, where the ranges of many understory cool-season grass species overlap. The experiment focused on seven of these grasses ( <i>Agrostis perennans</i> , <i>Elymus villosus</i> , <i>Elymus virginicus</i> , <i>Festuca subverticillata</i> , <i>Lolium arundinaceum</i> , <i>Poa alsodes</i> , and <i>Poa sylvestris</i> ), each of which hosts a unique species of <i>Epichloë</i> endophyte (Table S1). All are native to eastern North America except the Eurasian species <i>L. arundinaceum</i> .	215
	216
	217
	218
	219
	220
	221
	222
	223
	224
	225
<b>Endophyte removal, plant propagation, and field set-up</b>	226
Seeds from naturally symbiotic populations of the seven focal host species were collected during summer-fall 2006 from Lilly-Dickey Woods and the nearby Bayles Road Teaching and Research Preserve (39.220167, -86.542683). To generate symbiotic (S+)	227
	228
	229
	230

231 and symbiont-free (S-) plants from the same genetic lineages, seeds from each species  
232 were disinfected with a heat treatment described in Table S1 or left untreated. The heat  
233 treatment created symbiont-free plants by warming seeds to temperatures at which the  
234 fungus becomes inviable but the host seeds can still germinate. Both heat-treated and  
235 untreated seeds were surface sterilized with bleach to remove epiphyllous microbes,  
236 cold stratified for up to 4 weeks, then germinated in a growth chamber before transfer  
237 to the greenhouse at Indiana University where they grew for ~ 8 weeks. We confirmed  
238 endophyte status by staining thin sections of inner leaf sheath with aniline blue and  
239 examining tissue for fungal hyphae at 200X magnification [33]. We established exper-  
240 imental populations with vegetatively propagated clones of similar sizes. By starting  
241 the experiment with plants of similar sizes and the same number of unique genotypes,  
242 we aimed to limit any potential effects of heat treatments on initial plant growth [34].

243 During the fall of 2007 and spring of 2008, we established 10 3x3 m. plots for *A.*  
244 *perennans*, *E. villosus*, *E. virginicus*, *F. subverticillata*, and *L. arundinaceum* and 18  
245 plots for *P. alsodes* and *P. sylvestris*. Half of the plots were randomly assigned to be  
246 planted with either symbiotic (S+) or symbiont-free (S-) plants, and initiated with  
247 20 evenly spaced individuals labeled with aluminum tags. In spring 2008, we placed  
248 plastic deer net fencing around each plot to limit deer herbivory and disturbance;  
249 damaged fences were regularly replaced.

250

## 251 **Long-term demographic data collection**

252

253 Each summer (2008–2021) we censused all individuals in each plot for survival,  
254 growth and reproduction, and added new recruits to the census. Plots contained 13.3  
255 individuals/m<sup>2</sup> on average over the course of the experiment. Each census year was a  
256 sample of inter-annual climatic variation (n = 14 years, comprising 13 demographic  
257 transition years). We censused each species during its peak fruiting stage (May: *Poa*  
258 *alsodes*, *Poa sylvestris*; June: *Festuca subverticillata*; July: *Elymus villosus*, *Elymus vir-*  
259 *ginicus*, *Lolium arundinaceum*; September: *Agrostis perennans*), such that the censuses  
260 were pre-breeding and new recruits came from the previous years' seed production.  
261 Leaf litter was cleared out of each plot prior to the census, to aid in locating plants.  
262 For each plant remaining from the previous year, we determined survival, measured  
263 its size as a count of tillers, and collected reproductive data as counts of reproductive  
264 tillers and seed-bearing spikelets on all reproductive tillers to a maximum of three. We  
265 also tagged all unmarked individuals that were recruits from the previous years' seed  
266 production and collected the same demographic data. New recruits typically had one  
267 tiller and were non-reproductive. In 2008 through 2010, we took additional counts of  
268 seeds per inflorescence for all reproducing individuals in the plots to relate inflorescence  
269 and spikelet counts to seed production. In 2018, we stopped collecting data for the  
270 exotic *L. arundinaceum*, which had very high survival and low recruitment, and conse-  
271 quently very low variation across years. In total across 14 years, the dataset included  
272 demographic information for 16,789 individual host-plants and 31,216 transition-year  
273 observations.

274 We expected plots to maintain their endophyte status (symbiotic or symbiont-  
275 free) because these fungal symbionts are almost exclusively vertically transmitted,  
276 and plots were spaced a minimum of 5 m apart, limiting seed dispersal or horizontal

transmission of the symbiont between plots. However, we regularly confirmed endophyte treatment throughout the lifetime of the experiment by opportunistically taking subsets of seeds from reproductive individuals and scoring them for their endophyte status with microscopy as above. Overall, these scores reflected 98% faithfulness of recruits to their expected endophyte status across species and plots (Fig. S23; Supplement data). Additionally, we have rarely observed fungal stromata, the fruiting bodies by which *Epichloë* are potentially transmitted horizontally, provided the fly vector is also present [35]. For *A. perennans*, *F. subverticillata*, *L. arundinaceum*, and *P. alsodes*, we never observed stromata. We observed stromata only infrequently for *E. villosus*, and even more rarely for *E. virginicus* and *P. sylvestris* (Table S2). For these species, stromata have only been observed irregularly across years on 35, 4, and 6 plants respectively, making up < 0.3% of all censused plants.

## Vital rate modeling

Equipped with these demographic data, we fit statistical models for survival, growth, flowering (yes or no), fertility of flowering plants (number of flowering tillers), production of seed-bearing spikelets (number per inflorescence), the average number of seeds per spikelet, and the recruitment of seedlings from the preceding year's seed production. We fit these vital rates as generalized linear mixed models in a hierarchical Bayesian framework using RStan [36] which allowed us to isolate endophyte effects on vital rate means and variances, borrow strength across species for some variance components, and propagate uncertainty from the individual-level vital rates to population projection models [37]. All vital rate models included random plot and year effects, with separate estimates of year-to-year variance for symbiotic and symbiont-free plants, to quantify the effect of endophytes on inter-annual variance. All parameters were given vague priors [38]. We ran each vital rate model for 2500 warm-up and 2500 MCMC sampling iterations with three chains. We assessed model convergence with trace plots of posterior chains and checked for  $\hat{R}$  values less than 1.01, indicating low within- and between-chain variation [39, 40]. For those models that showed poor convergence, we extended the MCMC sampling to include 5000 warm-up and 5000 sampling iterations, which was only necessary for seedling growth. We graphically checked vital rate model fit with posterior predictive checks comparing simulated and observed data (Fig. S19-S20).

*Survival* - We modeled survival as a Bernoulli process, where the survival ( $S$ ) of an individual  $i$  in plot  $p$  and census year  $t$  was predicted by the plot-level endophyte status ( $e$ ), host species ( $h$ ), size in the preceding census, and the plant's origin status (whether it was initially transplanted or naturally recruited into the plot).

$$S_{i,p,e,h,t} \sim Bernoulli(\hat{S}_{i,p,e,h,t}) \quad (2a)$$

$$\text{logit}(\hat{S}_{i,p,e,h,t}) = \beta_{0_h} + \beta_1 * \text{origin}_i \quad (2b)$$

$$+ \beta_{2_h} * \text{endo}_e + \beta_{3_h} * \text{size}_{i,t-1} + \tau_{e,h,t} + \rho_p \quad (2c)$$

$$\tau_{e,h,t} \sim Normal(0, \sigma_{\tau_{e,h}}^2) \quad (2d)$$

323  $\rho_p \sim Normal(0, \sigma_\rho^2)$  (2e)  
 324

325 Here,  $\hat{S}$  is the survival probability,  $\beta_{0_h}$  is an intercept specific to each host species,  
 326  $\beta_1$  is the effect of the plant's recruitment origin,  $\beta_{2_h}$  is the endophyte effect,  $\beta_{3_h}$  is the  
 327 size effect,  $\tau_{e,h,t}$  is a normally distributed year effect for each species and endophyte  
 328 status with variance  $\sigma_{\tau_{e,h}}^2$ , and  $\rho_p$  is a normally distributed plot effect with variance  
 329  $\sigma_\rho^2$  ( $p(e)$  indicates that plot identity is uniquely associated with an endophyte status).  
 330 We assume that origin effect  $\beta_1$  and plot-to-plot variance  $\sigma_\rho^2$  are shared across host  
 331 species, allowing us to "borrow strength" across the multi-species dataset; other model  
 332 parameters are unique to host species. We separately modeled the survival of newly  
 333 recruited seedlings with a similar model but omitting previous size dependence and  
 334 origin status.

335 *Growth* - We modeled plant size in census year  $t$  ( $G$ ) with the same linear pre-  
 336 dictor for the mean as described for survival. Because we measured size as positive  
 337 integer-valued counts of tillers, we modeled it with a zero-truncated Poisson-inverse  
 338 Gaussian distribution. This distribution includes a shape parameter  $\lambda_G$  to account for  
 339 overdispersion in the data. We additionally modeled the growth of newly recruited  
 340 seedlings separately with a Poisson-inverse Gaussian model omitting size structure  
 341 and the plants' origin status as with seedling survival.

342 *Flowering* - We modeled whether or not a plant was flowering during the census ( $P$ )  
 343 as a Bernoulli process, with the same linear predictor for the mean as described above  
 344 for survival except that size dependence for reproductive vital rates was determined  
 345 by the individual's size during the same census year as opposed to its size during the  
 346 previous year.

347 *Fertility* - For a plant that was flowering during the census, its fertility was the  
 348 number of reproductive tillers produced ( $F$ ), which we modeled as a function of size in  
 349 the same census period with a zero-truncated Poisson-Inverse Gaussian distribution,  
 350 with the same linear predictor for the mean as described above.

351 *Spikelets per Inflorescence* - Spikelet production ( $K$ ) was recorded as integer counts  
 352 on up to three inflorescences per reproducing plant. We modeled these data with a neg-  
 353 ative binomial distribution, with the same linear predictor for the mean as described  
 354 above.

355 *Seed Production per Spikelet* - For individuals with recorded counts of seed pro-  
 356 duction, we calculated the number of seeds per spikelet from our counts of seeds and  
 357 spikelets per inflorescence, and then modeled seeds per spikelet ( $D$ ) as means of a  
 358 Gaussian distribution for each species and endophyte status. Because we had less  
 359 detailed data across years and plants for seed production than for other reproductive  
 360 vital rates, we omitted both plot and year random effects.

361 *Seedling Recruitment* - We used a binomial distribution to model the recruitment of  
 362 new seedlings ( $R$ ) into the plots from seeds produced in the preceding year, assuming  
 363 no long-lived seed bank. We included an intercept specific to each host and endophyte  
 364 status and the same random effects structure as in other models. We estimated the  
 365 number of seeds per plot in the preceding year by multiplying the total number of  
 366 reproductive tillers per plant by the mean number of spikelets per inflorescence and  
 367 mean number of seeds per spikelet ( $D$ ). For plants with missing fertility or spikelet

data, we used the expected number of reproductive tillers ( $F$ ) or of spikelets per inflorescence from ( $K$ ), drawing from the full posteriors of our models. We rounded this value to get the estimated seed production for each individual, and finally summed across all reproductive plants in each year and plot to get the total number of seeds produced.

## Stochastic population model

Using the fitted vital rate models, we parameterized stochastic matrix projection models including two state variables:  $r_t$  (the number of newly recruited individuals in year  $t$ ), and  $\mathbf{n}_t$  (a vector including all non-seedling individuals of sizes  $x \in \{1, 2, \dots, U\}$ , ranging from one to the maximum number of tillers  $U$ ). We use these two state variables to avoid having to assume demographic equivalence between seedling and non-seedling one-tiller plants. We used the same model structure for each species and endophyte status (not shown in model notation, to make it more readable).

The number of recruits in year  $t + 1$  is given by:

$$r_{t+1} = \sum_{x=1}^U P(x; \boldsymbol{\tau}_P) F(x; \boldsymbol{\tau}_F) K(x; \boldsymbol{\tau}_K) D R(\boldsymbol{\tau}_R) n_t^x \quad (3)$$

The total number of seeds produced by a maternal plant of size  $x$  is the product of the size-specific probability of flowering  $P$ , the number of reproductive tillers  $F$ , the number of spikelets per inflorescence  $K$ , and the number of seeds per spikelet  $D$ . Multiplying by the probability of transitioning from seed to seedling  $R$  gives a per-capita rate of seedling production, which is multiplied by the number of plants of size  $x$  ( $n_t^x$ , the  $x^{\text{th}}$  element of  $\mathbf{n}_t$ ) and summed over all sizes. Each function also depends on the species- and endophyte-specific year random effects for that vital rate ( $\boldsymbol{\tau}$ , a vector of year-specific values derived from the statistical models).

The number of  $y$ -sized plants in year  $t + 1$  is given by:

$$n_{t+1}^y = Z(y; \boldsymbol{\tau}_Z) B(\boldsymbol{\tau}_B) r_t + \sum_{x=1}^U S(x; \boldsymbol{\tau}_S) G(x, y; \boldsymbol{\tau}_G) n_t^x \quad (4)$$

where  $n_{t+1}^y$  is the  $y^{\text{th}}$  element of vector  $\mathbf{n}_{t+1}$ . The first term on the right hand side of Eqn. 4 represents growth ( $Z$ ) and survival ( $B$ ) of seedling recruits. The second term includes the survival of previously  $x$ -sized plants and the growth of survivors from size  $x$  to  $y$ , summed over all  $x$ . To avoid predictions of unrealistic growth outside of the observed size distribution, we set a ceiling on the growth function for plants at the 97.5<sup>th</sup> percentile of observed sizes for each host species [41].

Each of the vital rate functions in Eqns. 3 and 4 have separate intercepts and year random effects for symbiotic and symbiont-free populations, allowing us to calculate the effect of endophyte symbiosis on the mean, variance, and coefficient of variation (CV) of  $\lambda$ , the dominant eigenvalue of the year- and endophyte-specific projection matrix. This model treats climate drivers implicitly through year-specific random effects. We also developed a climate-explicit version with the addition of parameters defining the relationship between either annual or growing season drought index and

415 each vital rate. A full description of climate-explicit methods can be found in the  
416 *Supporting Information Supplemental Methods*.

417

## 418 Life History Analysis

419

420 We collected metrics describing each host species' life history to test the relationship  
421 between pace of life and variance buffering (Table S1). Using the Rage package [42], we  
422 calculated  $R_0$ , longevity, and generation time from our estimated transition matrices  
423 using the symbiont-free mean matrix as the reference condition. We recorded seed  
424 size as the average lemma length from the Flora of North America [43]. We also  
425 calculated the 99th percentile of maximum observed age for each species from their  
426 S- populations. Next, we fit Bayesian phylogenetic mixed-effects models using the  
427 brms package [44] to test the relationship between each life history trait and the  
428 effect of symbiosis on the CV of  $\lambda$  (a measure of variance buffering) while controlling  
429 for phylogenetic non-independence between host and symbiont species. We pruned  
430 species-level phylogenies of plants [45] and *Epichloë* fungi [46] to include the focal  
431 species. *Agrostis perennans* was not included in the tree, and so we used the congener  
432 *A. hyemalis*. We defined separate phylogenetic covariance matrices for each pruned  
433 tree. We propagated uncertainty in the estimated variance buffering effect  $V$  with a  
434 measurement error model:

435

436

$$V_{MEAN,h} \sim Normal(V_{EST,h}, V_{SD,h}) \quad (5a)$$

438

$$V_{EST,h} \sim Normal(\mu_h, \sigma) \quad (5b)$$

439

$$\mu = \alpha + \beta * trait + \pi_j \quad (5c)$$

440

$$\alpha \sim Normal(0, .5) \quad (5d)$$

441

$$\beta \sim Normal(0, .1) \quad (5e)$$

442

$$\sigma \sim Half-Normal(.04, .01) \quad (5f)$$

443

$$\pi_h \sim MVN(0, \sigma_\pi \mathbf{A}) \quad (5g)$$

444

$$\sigma_\pi \sim Half-Normal(0, .1) \quad (5h)$$

445

446

447 Here,  $V_{EST}$  is the variance buffering effect for host species  $h$ , estimated from the  
448 posterior mean ( $V_{MEAN}$ ) and standard deviation ( $V_{SD}$ ), propagating uncertainty asso-  
449 ciated with the effect of symbiosis. The model includes an intercept ( $\alpha$ ) and a slope  
450 ( $\beta$ ) defining the relationship between the variance buffering effect and the life history  
451 trait. The residual standard deviation is given by ( $\sigma$ ). We used weakly informative  
452 priors to aid model convergence. Each prior was centered at zero, except for the resid-  
453 ual standard deviation, which we centered at the standard deviation of the estimated  
454 variance buffering effect, .04. The phylogenetic random effect ( $\pi$ ), which is modeled  
455 as a multivariate normal distribution, has a between-species standard deviation ( $\sigma_\pi$ )  
456 structured by the phylogenetic covariance matrix  $\mathbf{A}$ . We ran each MCMC sampling  
457 chain for 8000 warmup iterations and 2000 sampling iterations. We assessed model  
458 convergence as described for the vital rate models.

459

460

<b>Mean-variance decomposition</b>	461
To calculate stochastic population growth rates ( $\lambda_s$ ) for each host species and endophyte status we simulated population dynamics for 1000 years by randomly sampling from the 13 annual transition matrices, discarding the first 100 years to minimize the influence of initial conditions. Sampling observed transition matrices produces models that realistically capture inter-annual variation by preserving correlations between vital rates [47]. We tallied the total population size at each time step as $N_t = r_t + \sum_{x=1}^U n_t^x$ and calculated the stochastic growth rate as $\log(\lambda_s) = E[\log(\frac{N_t}{N_{t+1}})]$ [48, 49]. We calculated the total effect of endophyte symbiosis as the difference in $\lambda_s$ between S+ and S- populations. We propagated uncertainty from the vital rate models to the calculation of $\lambda_s$ using 500 draws from the posterior distribution of model parameters.	462 463 464 465 466 467 468 469 470 471 472 473 474 475 476 477 478 479 480 481 482 483 484 485 486 487 488 489 490 491 492 493 494 495 496 497 498 499 500 501 502 503 504 505 506
We decomposed the total endophyte effect on $\lambda_s$ into contributions from effects on vital rate means, variances, and their interaction. Specifically, we repeated the calculation of $\lambda_s$ for two additional “treatments”: (1) endophyte effects on mean vital rates only, with inter-annual variances shared between S+ and S- at the S- reference level for all vital rates, and (2) endophyte effects on vital rate variances only, with vital rate means shared between S+ and S- at the S- reference level. The combination of all four $\lambda_s$ treatments (S+ vital rate means and variances, S- means and variances, S+ means with S- variances, S- means with S+ variances) allowed us to quantify to what extent the overall effect of symbiosis derives from changes in vital rates means, variances, and their interaction. The interaction occurs because the variance penalty to stochastic growth is proportional to the mean value of annual growth rates (see Eq. 1) such that variance is more detrimental for populations with lower average growth rates.	474 475 476 477 478 479 480 481 482 483 484 485 486 487 488 489 490 491 492 493 494 495 496 497 498 499 500 501 502 503 504 505 506
To create scenarios of increased variance relative to that observed during the study period, we repeated the stochastic growth rate decomposition, but sampling only a subset of the 13 observed annual transition matrices. We created two scenarios of increased environmental variance by sampling the transition matrices associated with the six or two most extreme $\lambda$ values, representing the six or two best and worst years, using S- populations as the reference condition. By sampling away from an average year in both directions, the six- and two- years scenarios increased the standard deviation of yearly host growth rates by 1.3 and 2.1 times, respectively, without changing mean growth rates (< 2.3% difference in $\bar{\lambda}$ between simulation treatments, Fig. S21). We performed the same mean-variance decomposition for these scenarios as for the ambient conditions (all 13 years sampled) for all host species described above.	487 488 489 490 491 492 493 494 495 496 497 498 499 500 501 502 503 504 505 506
<b>Results and Discussion</b>	499
<b>Symbionts buffer host demographic variance</b>	500
Across seven host species, eight vital rates, 14 years, and 16,789 individual plants, our analysis provided the first empirical evidence of symbiont-mediated variance buffering. Endophytes reduced inter-annual variance for 66% (37/56) of host species-vital rate combinations (average Cohen’s D for effects on vital rate standard deviation:	501 502 503 504 505 506

507 -0.15) (Fig 1A; Fig. S6 - Fig. S18). Endophytes also increased mean vital rates for  
508 the majority (36/56) of host species-vital rate combinations (average Cohen's D for  
509 effects on vital rate mean: 0.15), and benefits were particularly strong for host sur-  
510 vival, plant growth and recruitment (Fig. 1A; Fig. S1 - Fig. S5). The magnitude of  
511 mean and variance effects differed among host species and vital rates. For example,  
512 endophytes modestly increased mean adult survival (Fig. 1C) and reduced variance in  
513 survival (Fig. 1D) for *Festuca subverticillata*, while for *Poa alsodes*, variance buffer-  
514 ing was more apparent in seedling growth and inflorescence production (Fig 1E).  
515 Interestingly, certain vital rates showed costs of endophyte symbiosis. Symbiotic indi-  
516 viduals of *A. perennans* grew larger than those without endophytes (Fig. 1B), yet  
517 endophytes also reduced this species' mean recruitment rates (Fig. 1A). In addition,  
518 endophyte symbiosis increased variance in seedling growth for *Elymus villosus* and  
519 *Festuca subverticillata* (Fig. 1A).

520 Because not all vital rates contribute equally to fitness, we used stochastic matrix  
521 models to integrate the diverse effects on vital rates described above into comprehen-  
522 sive measures for the mean and variance of year-to-year fitness ( $\lambda_t$ ) and the long-run  
523 stochastic fitness that integrates both mean and variance ( $\lambda_S$ ). On average across host  
524 species, S+ populations had greater mean fitness (> 92% confidence that endophytes  
525 increased  $\bar{\lambda}$ ) and lower inter-annual variability in fitness (> 86% confidence that endo-  
526 phytes decreased the coefficient of variation of  $\lambda_t$ ) than S- populations (Fig. 2). For  
527 some host species, the CV of  $\lambda_t$  declined by as much as 170% (*P. alsodes*, *F. subverti-*  
528 *cillata*), while for others, endophyte effects on variance were substantially smaller (6%  
529 lower for *E. villosus*, 16% lower for *A. perennans*), or even positive (27% increase for  
530 *E. virginicus*). When mean and variance effects of symbionts were considered together,  
531 none of the host-symbiont pairings were antagonistic (i.e., with endophytes that both  
532 decreased mean fitness and increased variance) (Fig. 2C), suggesting that variation  
533 across host species and vital rates in mean and variance effects may reflect alternative  
534 strategies that yield similar net benefits of endophyte symbiosis.

535 Reduced sensitivity to drought, as has been reported for some *Epichloë* symbioses  
536 [32], is a candidate mechanism that could generate a signature of variance buffering:  
537 drought conditions may have weaker fitness costs for S+ hosts, reducing fluctuations in  
538 fitness through time. Accordingly, analysis of climate-explicit matrix models indicated  
539 that, for five of seven taxa, S+ populations were less sensitive to annual or growing  
540 season drought (12-month or 3- month drought index; Standardized Precipitation-  
541 Evapotranspiration Index [50]) than S- populations (Supporting Information Text;  
542 Fig. S24-S25; Table S3). However, we did not find a strong relationship between the  
543 magnitude of variance buffering and relative drought sensitivities, suggesting that  
544 other climatic factors or other temporally-varying aspects of the environment may  
545 elicit benefits of endophyte symbiosis, including documented resistance to herbivory  
546 for six of these host taxa [51, 52].

547

#### 548 **Faster life histories predict stronger symbiont-mediated 549 variance buffering**

550

551 Theory predicts that long-lived species, those on the slow end of the slow-fast life  
552 history continuum, will be less sensitive to environmental variability than short-lived

species [53], a pattern which has empirical support across plants [54] and animals [8, 55]. Therefore, host species with long lifespans that produce few, large offspring should benefit less from symbiont-mediated variance buffering than species with fast life cycles that produce many smaller offspring with low per-capita chance of success [56, 57]. In support of this prediction, hosts with trait values representing faster life history strategies experienced greater variance buffering from endophytes than those with slow life histories (Fig. 3). Bayesian phylogenetic mixed-effects models, controlling for species' relatedness, indicated that variance buffering was stronger for host species with shorter lifespan (Fig. 3A; 75% probability of positive relationship with empirically observed maximum plant age) and smaller seeds (Fig. 3B; 73% probability of positive relationship with seed length). Other life history traits similarly had positive, but weaker, support for the prediction that faster life history traits correlate with stronger variance buffering (Fig. S26-S28). Considering fungal life history traits, the three host species for which the net mutualism benefit was weakest (*Elymus villosus*, *Elymus virginicus*, and *Poa sylvestris*) (Fig. 2C) were the only hosts for which we observed fungal stromata, fruiting bodies capable of horizontal (contagious) transmission (Table S2). This result supports the theoretical expectation that strict vertical transmission drives the evolution of strong host-symbiont mutualism [20, 58]. Conclusions about life histories are somewhat constrained by the narrow range of trait values among closely related species in the grass sub-family Pooideae and their co-evolving symbionts. Our understanding of how life history variation modulates the fitness consequences of microbial symbiosis would profit from tests across a wider span of taxonomic groups [59].

## Contributions from variance buffering are weak relative to mean effects

To evaluate the relative importance of mean fitness benefits and variance buffering as alternative pathways of mutualism, we decomposed the overall effect of the symbiosis on the stochastic growth rate  $\lambda_S$  using simulations from the population models in four configurations. These included either the full symbiosis effect (both mean and variance buffering effects), mean effects alone, variance effects alone, or neither mean nor variance effects. Overall, the full effect of symbiosis on  $\lambda_S$ , averaged across host species, provided strong evidence of grass-endophyte mutualism (99% certainty of a positive total effect on  $\lambda_s$ ) (Fig. 4; see Fig. S22 for individual host species). Contributions to this full effect derived from both mean and variance buffering effects, as well as a slightly negative interaction (i.e., the combined influence of mean and variance effects was smaller than the sum of their individual effects). Endophytes' contributions to  $\lambda_S$  from mean effects were four times greater, averaged across species, than contributions from variance buffering (Fig. 4), suggesting that, under the regime of environmental variability represented by our 14-year study, damped fluctuations in fitness via variance buffering was a far less important element of the benefits of symbiosis than increased mean fitness. Results for individual host species were largely consistent with the cross-species trends (Fig S22). The full effect of symbiosis on  $\lambda_S$  was positive for seven out of eight host species, with statistical confidence ranging from 66% to > 99% certainty. The one exception was the host species *P. sylvestris*, for which our analysis

599 indicated that fungal endophytes were effectively neutral in their overall fitness effect  
600 (45% and 55% posterior probability of positive and negative effects; Fig S22).

601

## 602 **Variance buffering strengthens under increased environmental 603 variability**

604

605 Simulations of increased environmental variability, a key prediction of climate change  
606 forecasts [2], indicated that mutualism with microbial symbionts, and their variance  
607 buffering effects in particular, will take on increased importance for hosts in a more  
608 variable future climate. To simulate increased variability, we repeated the decomposi-  
609 tion of  $\lambda_S$  for two alternative forecast scenarios, randomly sampling transition matrices  
610 that represented either the six most extreme years experienced by each species or the  
611 two most extreme years, subsets of the thirteen transition matrices across the 14-year  
612 study period. Increased variability elicited stronger mutualistic benefits of endophyte  
613 symbiosis (Fig. 3) than ambient variability (overall effect of the symbiosis increased  
614 by > 130%). This increase was driven by increased contributions from the variance  
615 buffering mechanism (from a 24% contribution in the ambient scenario to a 66% con-  
616 tribution in the most variable scenario) rather than from greater mean effects. In the  
617 most variable scenario, the relative importance of mean and variance effects reversed,  
618 with variance buffering contributions that were 1.5 times greater than contributions  
619 from mean benefits, averaged across species (Fig. 4). Thus, variance buffering – a cryp-  
620 tic microbial influence that manifests only over long time scales – is poised to become  
621 the dominant way in which grasses benefit from symbiosis with fungal endophytes in  
622 more variable climates of the future.

623

## 624 **Conclusion**

625

626 Ecologists increasingly recognize the importance of symbiotic microbes for host organ-  
627 isms and the populations, communities, and ecosystems in which their hosts reside  
628 [60–63]. Despite awareness of these ubiquitous interactions, long-term studies of micro-  
629 bial symbiosis are very rare. Our analysis of taxonomically-replicated, long-term field  
630 experiments that manipulated the presence/absence of fungal symbionts in plants  
631 demonstrates for the first time that heritable microbes can commonly benefit hosts  
632 not only through improved mean fitness – the focus of most previous research – but  
633 also through buffering against environmental variance. Our results provide an impor-  
634 tant advance to improve forecasts of the responses of populations (and symbionts)  
635 to increasing environmental stochasticity under global change, suggesting that, for  
636 some host species, microbial symbiosis may compensate for the lack of intrinsic toler-  
637 ance of variability conferred by “slow” life history traits. We found that, relative to  
638 mean fitness benefits, symbiont-mediated variance buffering made weak contributions  
639 to host-symbiont mutualism under the current regime of environmental variability.  
640 However, variance buffering is likely to become the dominant benefit that fungal  
641 endophytes confer to grass hosts in more variable future environments. This result  
642 emerges from the context-dependent nature of grass-endophyte interactions, combined

643

644

with the observation that environmental stochasticity generates fluctuation in context. These key ingredients, and thus the potential for symbiont-mediated variance buffering, similarly apply to the diverse host-microbe symbioses across the tree of life. 645  
646  
647  
648  
649  
650  
651  
652  
653  
654  
655  
656  
657  
658  
659  
660  
661  
662  
663  
664  
665  
666  
667  
668  
669  
670  
671  
672  
673  
674  
675  
676  
677  
678  
679  
680  
681  
682  
683  
684  
685  
686  
687  
688  
689  
690

691 **Acknowledgments.** We thank Mark Sheehan, Ali Campbell, Kyle Dickens, Blaise  
692 Willis, and Sar Lindner for contributions to field data collection. We also thank Volker  
693 Rudolf, Daniel Kowal, Lydia Beaudrot and Judie Bronstein for helpful comments on  
694 and discussion of this project. This research was supported by the National Science  
695 Foundation (grants 1754468 and 2208857).

696 **Supplementary information.** Supplementary information for this paper includes  
697 Supplementary Methods, Figs. A1 to A28, and Tables A1 to A3.  
698

699

700

701

702

703

704

705

706

707

708

709

710

711

712

713

714

715

716

717

718

719

720

721

722

723

724

725

726

727

728

729

730

731

732

733

734

735

736

## Figures

737  
738  
739  
740  
741  
742  
743  
744  
745  
746  
747  
748  
749  
750  
751  
752  
753  
754  
755  
756  
757  
758  
759  
760  
761  
762  
763  
764  
765  
766  
767  
768  
769  
770  
771  
772  
773  
774  
775  
776  
777  
778  
779  
780  
781  
782

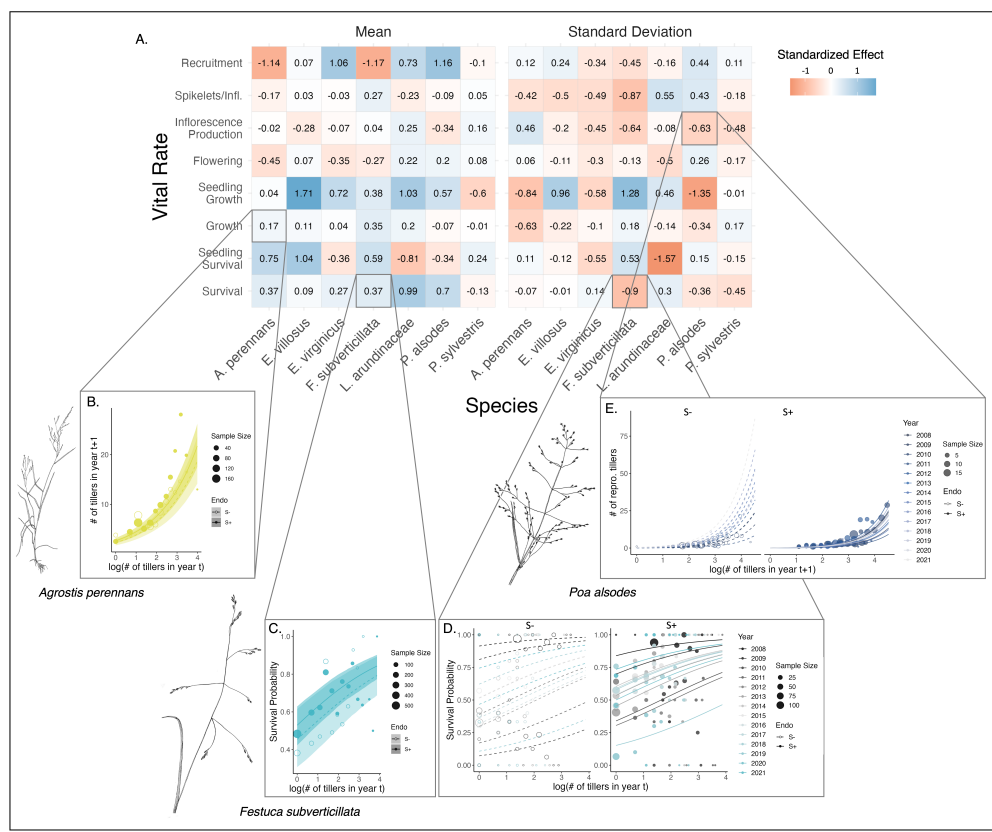
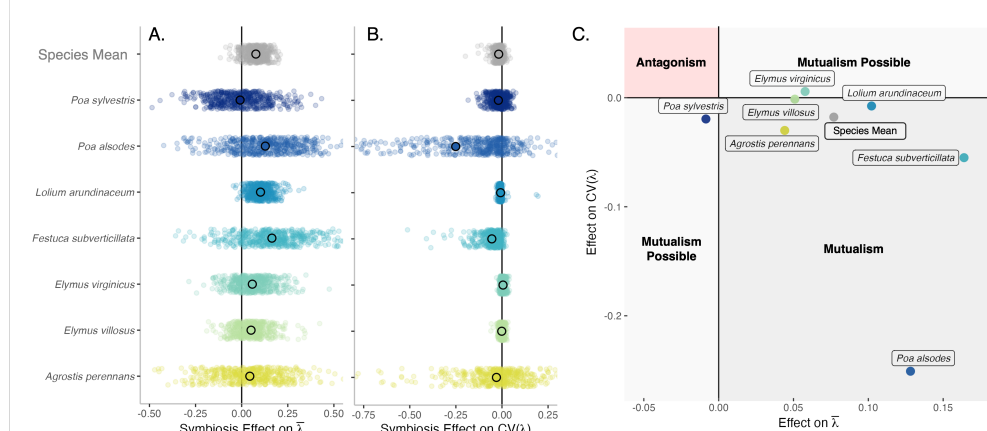


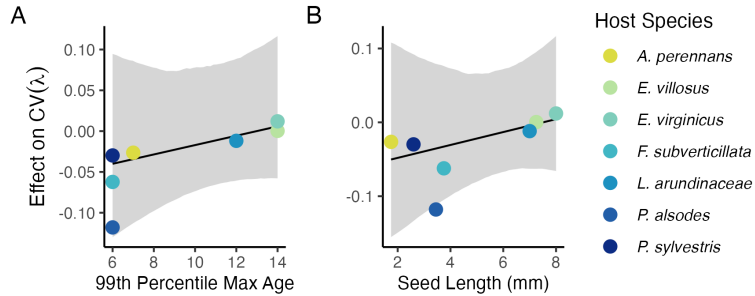
**Fig. 1** Endophyte symbiosis altered host vital rates.(A) Shading represents the posterior mean standardized effect size (Cohen's D) of endophyte symbiosis on mean or standard deviation of host vital rates (blue indicates that symbiosis increased the mean or standard deviation and red indicates a reduction). Endophytes' diverse vital rate effects include increased (B) mean growth of *A. perennans* and (C) mean survival probability of *F. subverticillata*. Endophyte presence also reduced inter-annual variance in (D) the survival of *F. subverticillata* and (E) the fertility of *P. alsodes*. In panels B-C, mean vital rate estimates are shown with 80% credibles along with data binned by size for symbiotic (S+) and symbiont-free (S-) plants, while in panels D-E, annual vital rate estimates are shown along with data binned by size and census year. Organism silhouettes modified from "Festuca subverticillata" by Cindy Roché and "Agrostis hyemalis" and "Poa alsodes" by Sandy Long ©Utah State University.

783  
784  
785  
786  
787  
788  
789  
790  
791  
792  
793  
794  
795  
796  
797  
798  
799



800  
801 **Fig. 2** Mean and variance-buffering effects on fitness. Black circles indicate the average effect of  
802 endophytes along with 500 posterior draws (smaller colored circles) on the (A) mean and (B) coeffi-  
803 cient of variation in  $\lambda$  for each host species as well as a cross species mean. (C) For all hosts,  
804 endophytes either reduce variance, increase the mean, or both, and consequently when considering  
805 stochastic environments, the interactions are always at least potentially mutualistic.

806  
807  
808  
809  
810  
811  
812  
813  
814  
815  
816  
817  
818  
819  
820  
821



822 **Fig. 3** Host species with faster life history traits experience stronger effects of symbiont-mediated  
823 variance buffering. Regressions between life history traits describing the fast-slow life history contin-  
824 uum ((A) 99th percentile maximum age observed during long term censuses in years; (B) Seed size)  
825 and the effect of endophyte symbiosis on the coefficient of variation in population growth rate ( $\lambda$ ).  
826 Each panel shows the fitted mean relationship (line) along with the 95% credible interval.  
827  
828

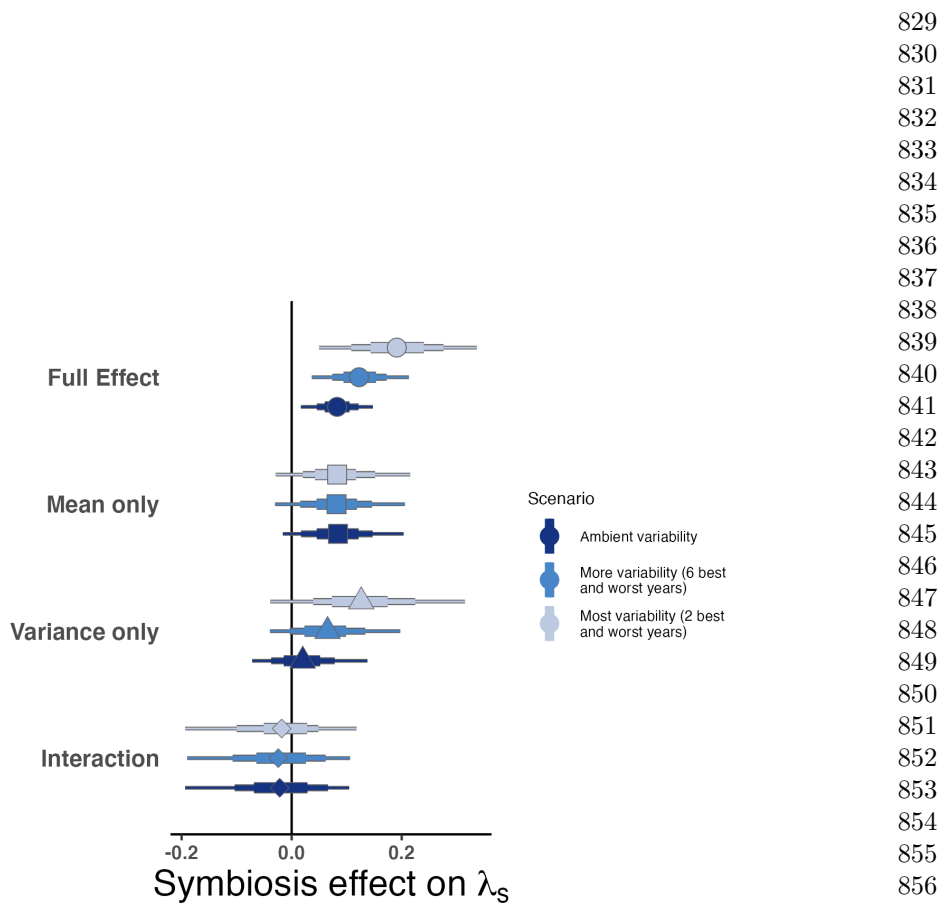


**Fig. 4** Cross-species average endophyte contributions to stochastic growth rates under observed and elevated variance. Endophyte symbiosis contributes to the total effect of mutualism on  $\lambda_S$  through benefits to mean growth rates and through variance buffering as well as the interaction between mean and variance effects. Shapes indicate the posterior mean of each contribution averaged across the seven focal symbiota, along with bars for the 50, 75 and 95% credible intervals. The full effect of the symbiosis (circles) becomes more mutualistic under scenarios of increased variance (represented by color shading). Relative to the ambient scenario sampling transition matrices for all 13 transition years during the study period, simulations increased variance by sampling the most extreme six or two years years, leading to increased contributions from variance buffering effects (triangles) and a constant contribution from mean effects (squares).

875 **Supporting Information**

876

877 **Supplemental Methods**

878 **Estimating climate drivers of environmental context-dependence**

879 To connect the variance buffering effects of endophytes with inter-annual variability  
880 in climate, we built climate-explicit stochastic matrix population models from the  
881 vital rate data in addition to the climate-implicit model described in the main text.  
882 Identifying the potentially complex relationships between vital rates and environmen-  
883 tal drivers remains a key challenge for accurate forecasts of the ecological impacts of  
884 environmental stochasticity [64]. We first downloaded temperature and precipitation  
885 data from a weather station in Bloomington, IN, approx. 27 km from our study site,  
886 using the rnoaa package [65]. Compared to other weather stations in the area, the  
887 measurements from Bloomington contain the most complete climate record across the  
888 study period and are correlated with more local measurements from Nashville, IN for  
889 years in which local data are available (total daily precipitation:  $R^2 = .76$ ; mean daily  
890 temperature:  $R^2 = .94$ ). The mean annual temperature across the study period was  
891  $11.9 C^\circ$  (SD:  $1.05 C^\circ$ ) and the average annual precipitation was  $1237.9 \text{ mm/year}$  (SD:  
892  $204.89 \text{ mm/year}$ ) (Fig. S24). Given the known role of endophytes in promoting host  
893 drought tolerance, we calculated the Standardised Precipitation-Evapotranspiration  
894 Index (SPEI) for 3 and 12 months preceding each annual censuses, reflecting drought  
895 during the growing season and across the year [50]. To calculate SPEI, we used the  
896 Thornthwaite equation to model potential evapotranspiration as implemented in the  
897 SPEI R package [66]

898 We repeated the process of fitting statistical models for each vital rate as described  
899 in **Materials and Methods** with the inclusion of a parameter describing the influ-  
900 ence of SPEI. We fit separate vital rate models incorporating either the growing season  
901 or annual drought index for each vital rate, except for the model describing the mean  
902 number of seeds per inflorescence. This model was fit without climate effects because  
903 the data came from only a few years. Initial analyses indicated similar fits for models  
904 including only a linear term and those with both linear and quadratic terms describ-  
905 ing the relationship between the climate driver and the vital rate response, and so  
906 we proceeded with models including only the linear term. We expected that includ-  
907 ing climate predictors into the models would explain some inter-annual variance in  
908 vital rates, shrinking the variance associated with the fitted year random effects. We  
909 assessed model fit with graphic posterior predictive checks and convergence diagnostics  
910 as described for the climate-implicit analysis. Finally, we next built matrix projec-  
911 tion models incorporating the climate-dependent vital rate functions to assess the  
912 response of symbiotic (S+) vs symbiont-free (S-) populations to drought. The model  
913 is as described in **Materials and Methods** with the inclusion of parameters describ-  
914 ing the slope of the relationship with SPEI. We compared the sensitivity of  $\lambda$  to either  
915 annual or seasonal SPEI of S+ populations ( $\frac{\Delta\lambda^+}{\Delta SPEI}$ ) with those of S- populations  
916 ( $\frac{\Delta\lambda^-}{\Delta SPEI}$ )(Fig. S25; Table S).

917 Most species were slightly more responsive to growing season rather than annual  
918 drought conditions, and for most species symbiotic populations were less sensitive to  
920

SPEI than symbiont-free populations (Fig. S25; Table S3). However, these drought indices did not explain the full extent of inter-annual variability in demographic vital rates. For example, flowering in <i>A. perennans</i> had one of the strongest climate signals (82% probability of a positive relationship with SPEI), yet the estimated inter-annual variance $\sigma_{\tau_P}^2$ for symbiont-free plants shrank from 6.7 to 6.1 after including 3-month SPEI as a covariate, suggesting that other factors contribute to inter-annual variability.	921
	922
	923
	924
	925
	926
	927
	928
	929
	930
	931
	932
	933
	934
	935
	936
	937
	938
	939
	940
	941
	942
	943
	944
	945
	946
	947
	948
	949
	950
	951
	952
	953
	954
	955
	956
	957
	958
	959
	960
	961
	962
	963
	964
	965
	966

## 967 Supplemental Figures S1-S28

968

969

970

971

972

973

974

975

976

977

978

979

980

981

982

983

984

985

986

987

988

989

990

991

992

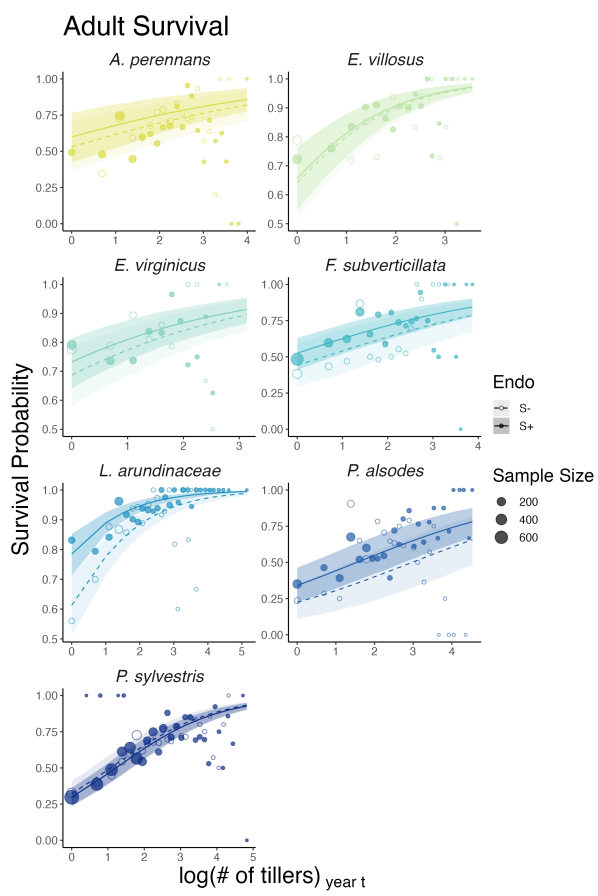
993

994

995

996

997



998 **Fig. S1** Effect of endophyte symbiosis on mean adult survival. Fitted curves represent the size-  
999 specific mean survival probability along with data binned by size shown as open circles with a dashed  
1000 line for symbiont-free (S-) plants, while the solid line and filled circles represent symbiotic (S+)  
1001 plants. 80% credible intervals are shown with dark shading for S+, or light shading for S-.

1002

1003

1004

1005

1006

1007

1008

1009

1010

1011

1012

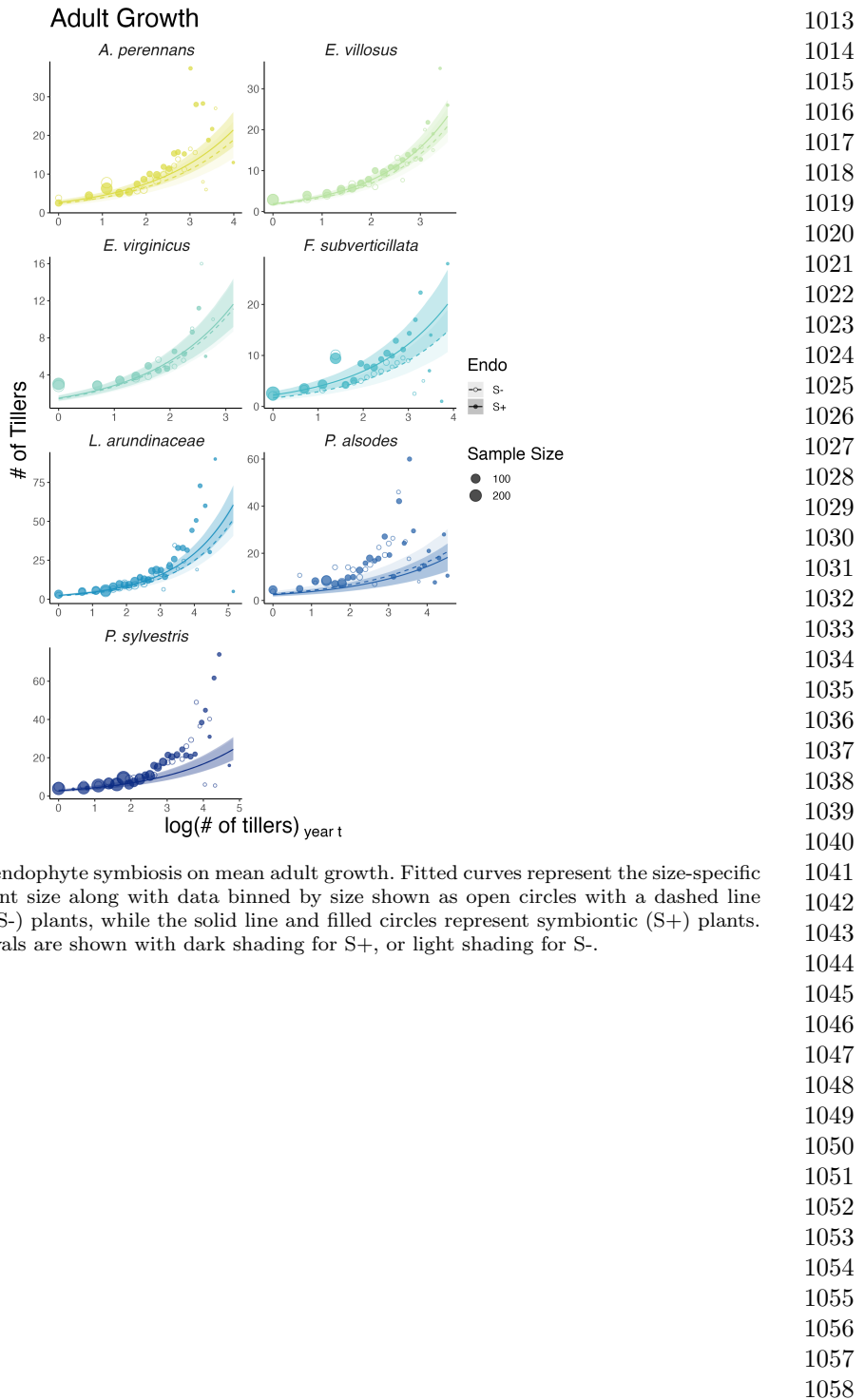
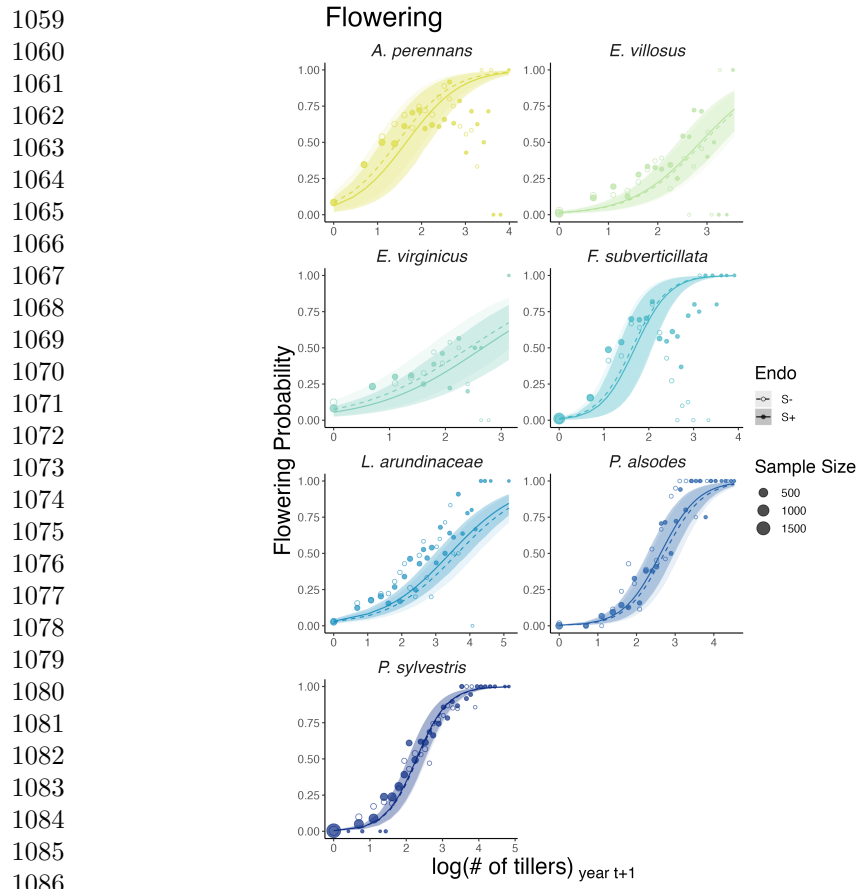


**Fig. S2** Effect of endophyte symbiosis on mean adult growth. Fitted curves represent the size-specific mean expected plant size along with data binned by size shown as open circles with a dashed line for symbiont-free (S-) plants, while the solid line and filled circles represent symbiotic (S+) plants. 80% credible intervals are shown with dark shading for S+, or light shading for S-.



1087 **Fig. S3** Effect of endophyte symbiosis on mean flowering. Fitted curves represent the size-specific  
1088 mean flowering probability along with data binned by size shown as open circles with a dashed line  
1089 for symbiont-free (S-) plants, while the solid line and filled circles represent symbiotic (S+) plants.  
1090 80% credible intervals are shown with dark shading for S+, or light shading for S-.

1091  
1092  
1093  
1094  
1095  
1096  
1097  
1098  
1099  
1100  
1101  
1102  
1103  
1104

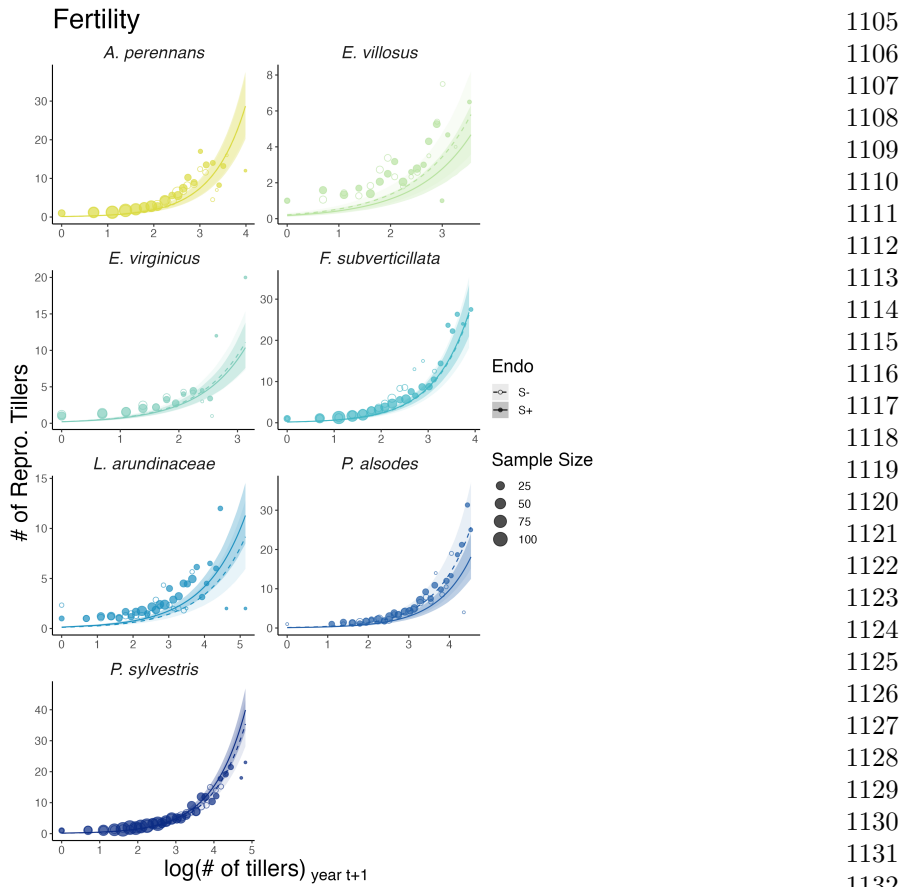
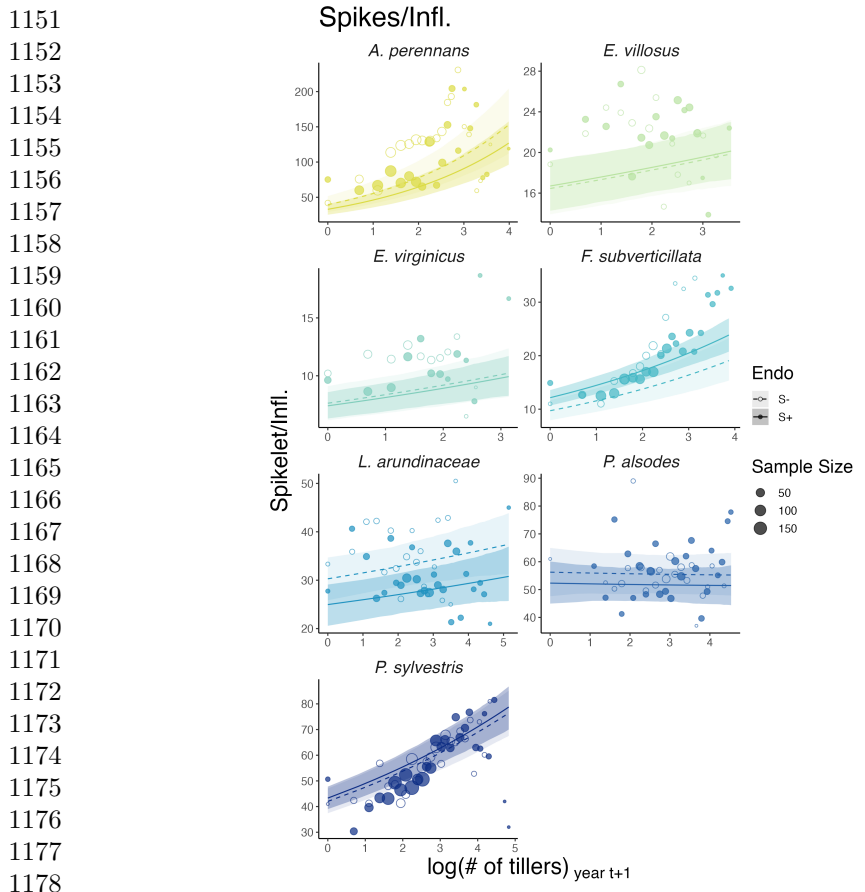


**Fig. S4** Effect of endophyte symbiosis on mean fertility. Fitted curves represent the size-specific mean expected number of flowering tillers along with data binned by size shown as open circles with a dashed line for symbiont-free (S-) plants, while the solid line and filled circles represent symbiotic (S+) plants. 80% credible intervals are shown with dark shading for S+, or light shading for S-.

1105  
1106  
1107  
1108  
1109  
1110  
1111  
1112  
1113  
1114  
1115  
1116  
1117  
1118  
1119  
1120  
1121  
1122  
1123  
1124  
1125  
1126  
1127  
1128  
1129  
1130  
1131  
1132  
1133  
1134  
1135  
1136  
1137  
1138  
1139  
1140  
1141  
1142  
1143  
1144  
1145  
1146  
1147  
1148  
1149  
1150



1179 **Fig. S5** Effect of endophyte symbiosis on mean spikelet production. Fitted curves represent the size-  
1180 specific mean expected number of spikelets per inflorescence along with data binned by size shown  
1181 as open circles with a dashed line for symbiont-free (S-) plants, while the solid line and filled circles  
1182 represent symbiotic (S+) plants. 80% credible intervals are shown with dark shading for S+, or light  
1183 shading for S-.

1183  
1184  
1185  
1186  
1187  
1188  
1189  
1190  
1191  
1192  
1193  
1194  
1195  
1196

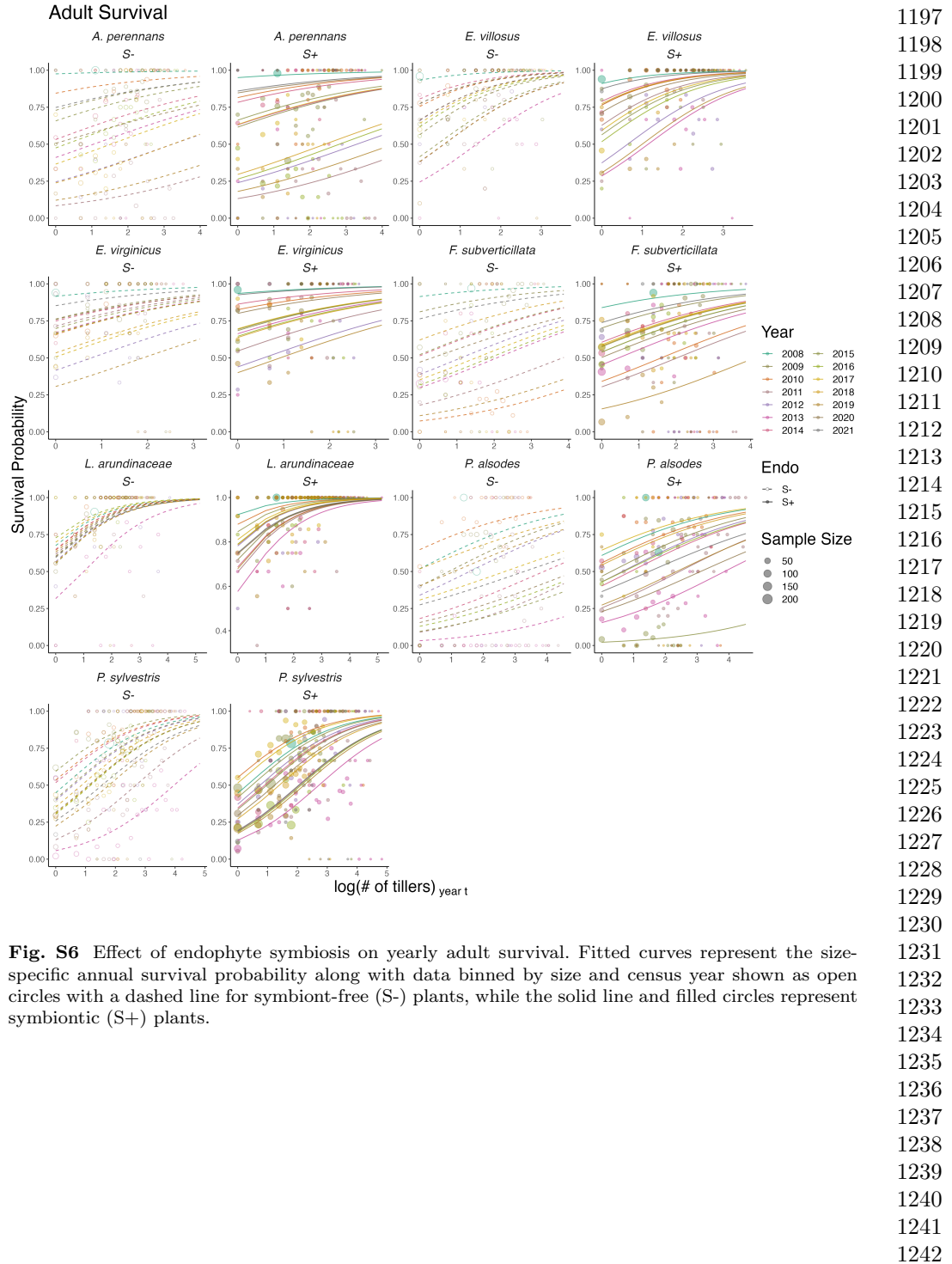
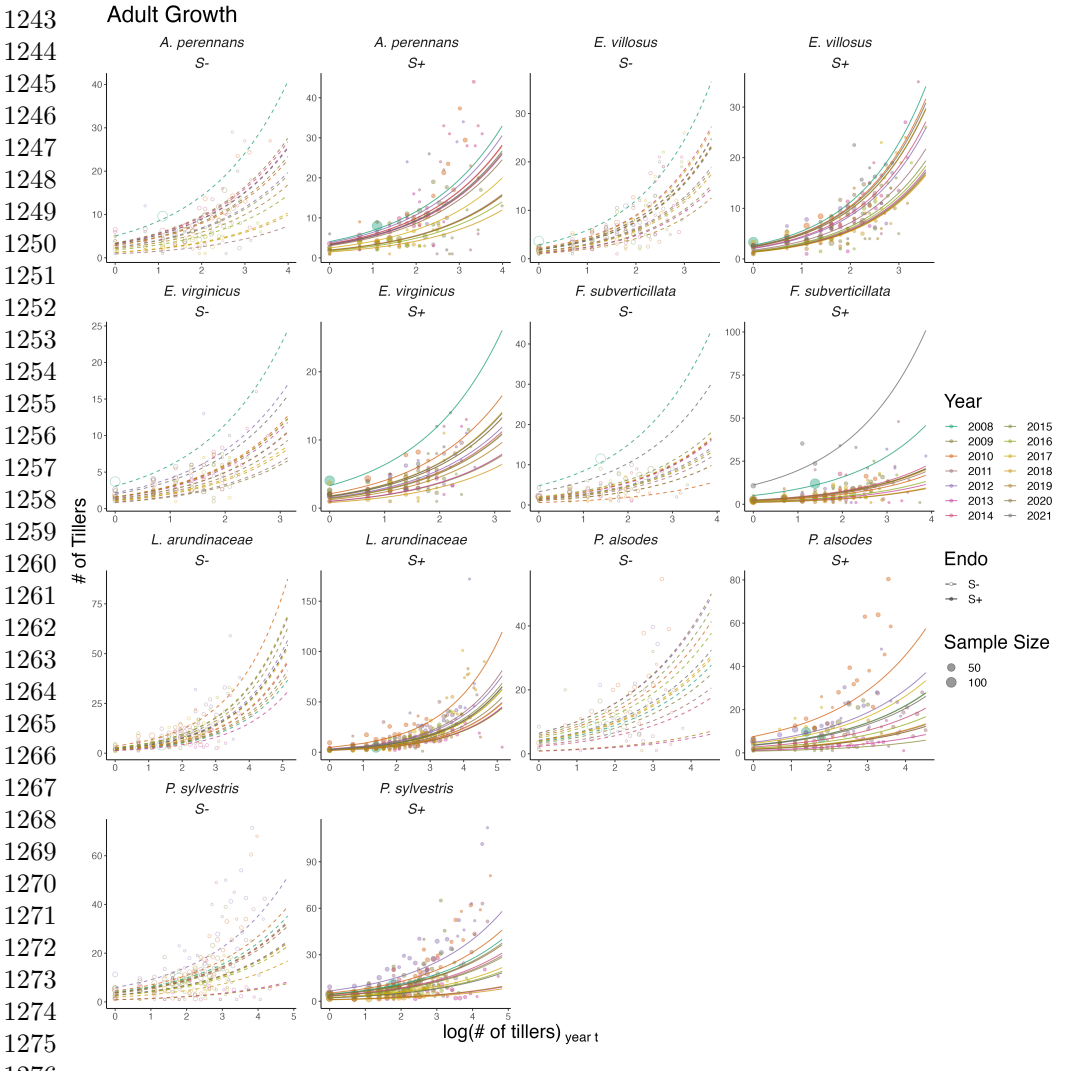
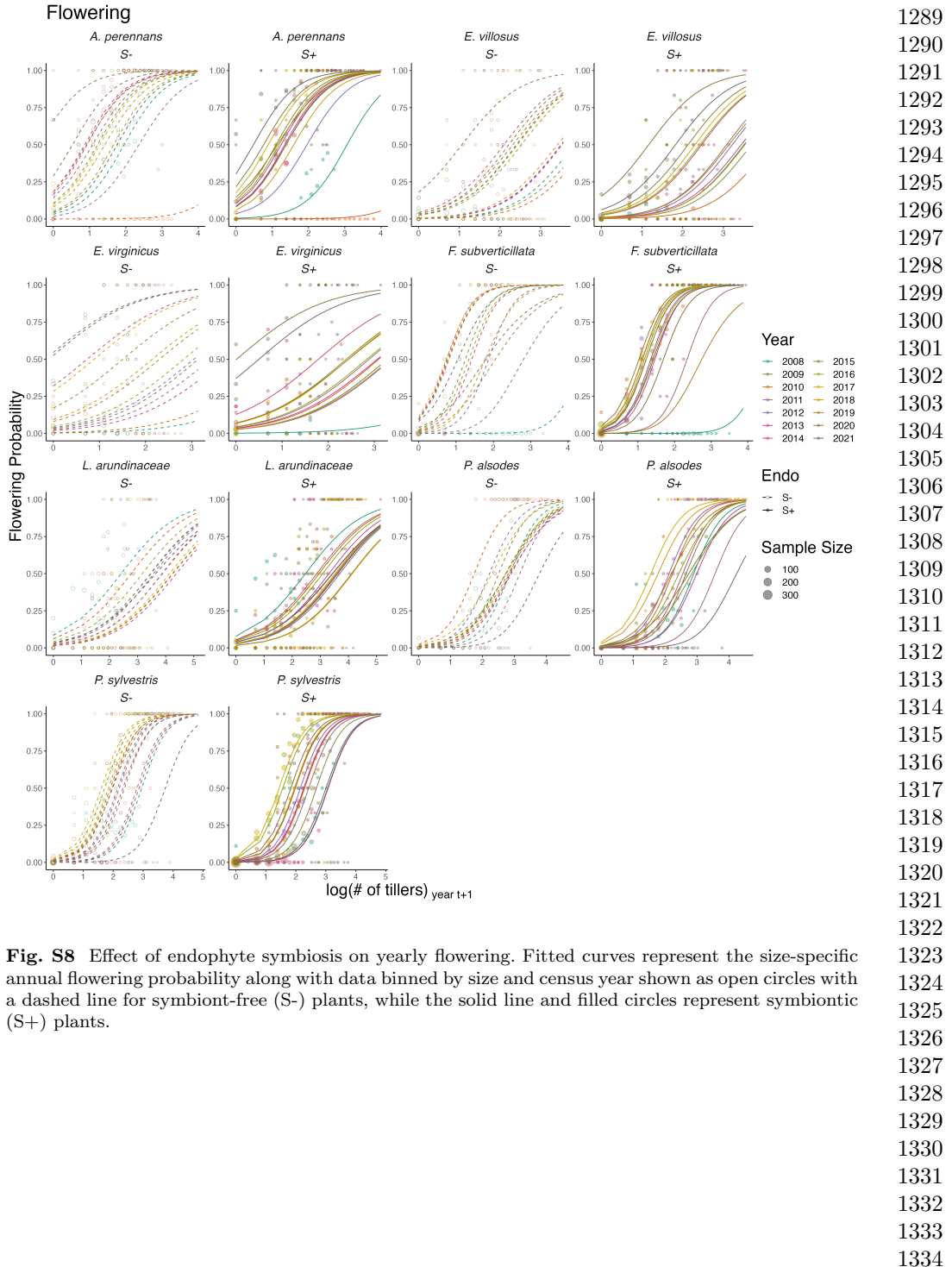


**Fig. S6** Effect of endophyte symbiosis on yearly adult survival. Fitted curves represent the size-specific annual survival probability along with data binned by size and census year shown as open circles with a dashed line for symbiont-free (S-) plants, while the solid line and filled circles represent symbiotic (S+) plants.

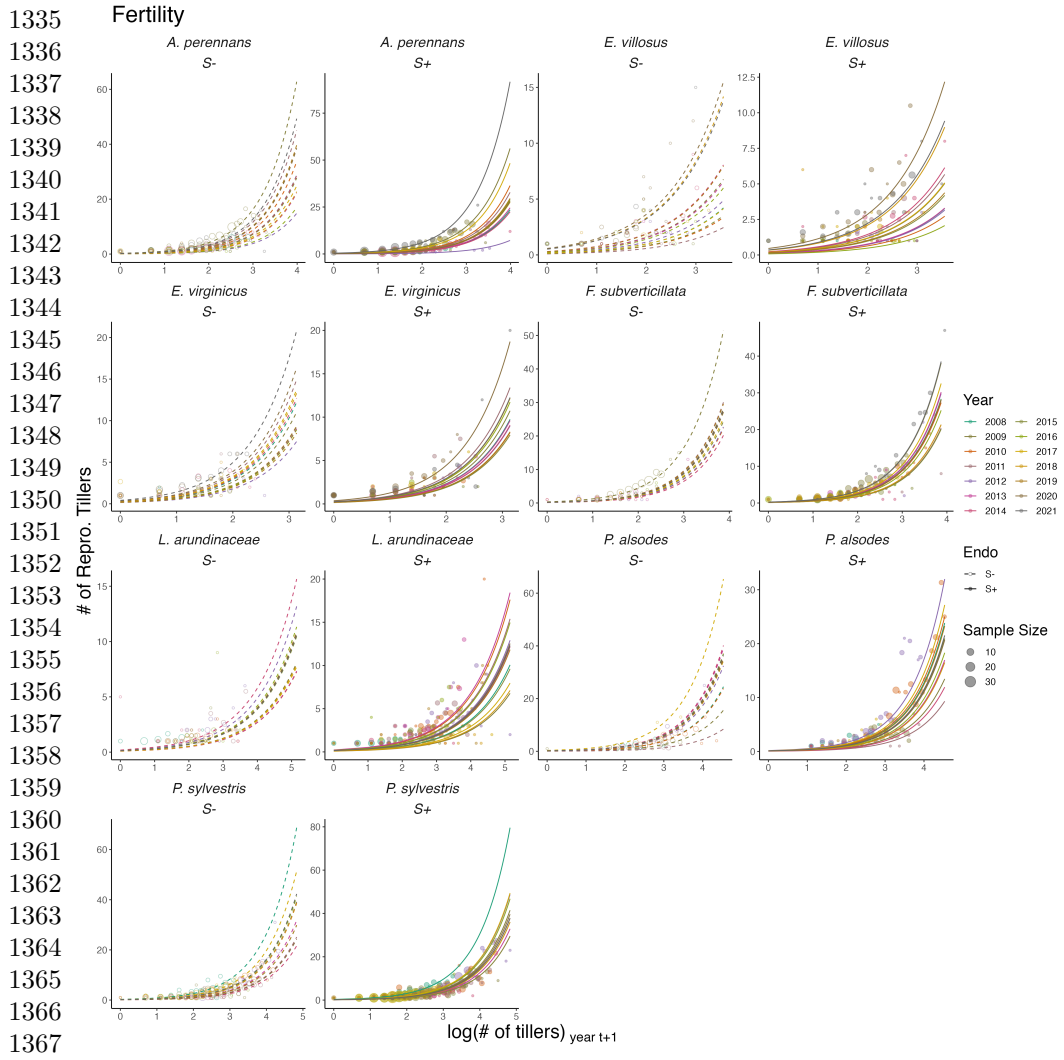


1277 **Fig. S7** Effect of endophyte symbiosis on yearly adult growth. Fitted curves represent the size-  
 1278 specific annual expected plant size along with data binned by size and census year shown as open  
 1279 circles with a dashed line for symbiont-free (S-) plants, while the solid line and filled circles represent  
 1280 symbiotic (S+) plants.

1281  
 1282  
 1283  
 1284  
 1285  
 1286  
 1287  
 1288



**Fig. S8** Effect of endophyte symbiosis on yearly flowering. Fitted curves represent the size-specific annual flowering probability along with data binned by size and census year shown as open circles with a dashed line for symbiont-free (S-) plants, while the solid line and filled circles represent symbiotic (S+) plants.



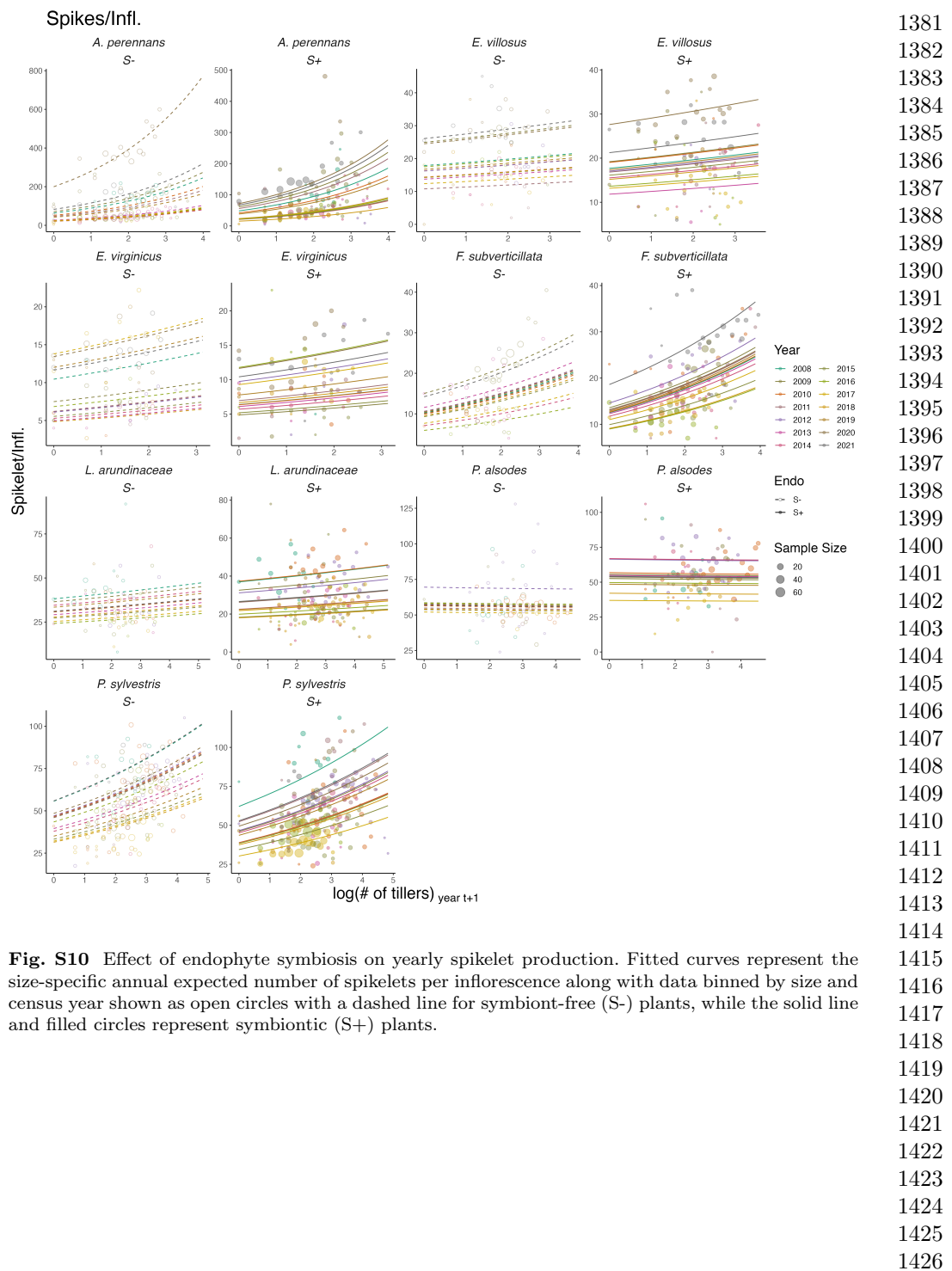
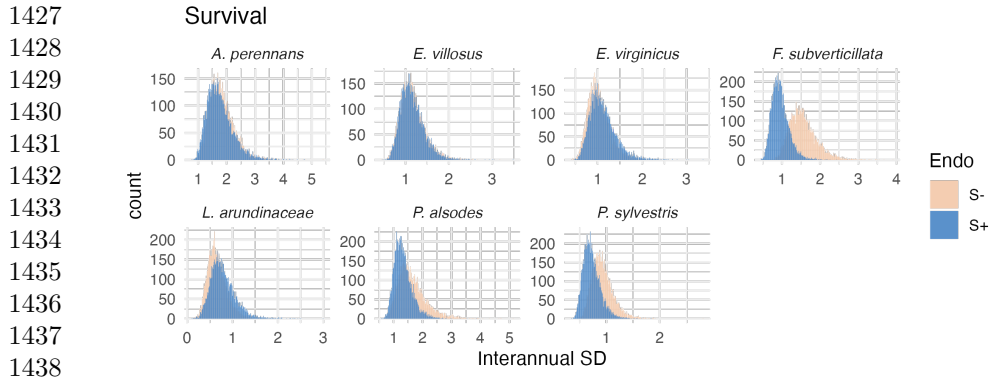
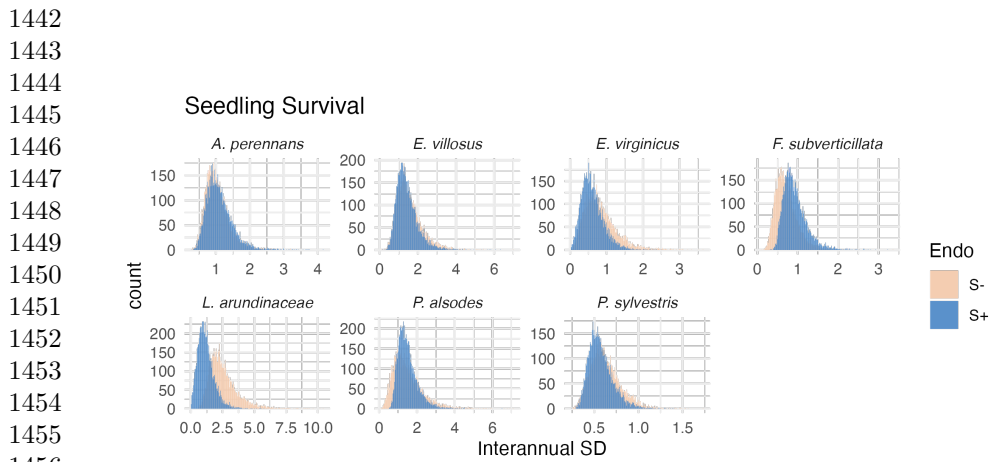


**Fig. S10** Effect of endophyte symbiosis on yearly spikelet production. Fitted curves represent the size-specific annual expected number of spikelets per inflorescence along with data binned by size and census year shown as open circles with a dashed line for symbiont-free (S-) plants, while the solid line and filled circles represent symbiotic (S+) plants.



1439 **Fig. S11** Posterior distributions of the standard deviations of inter-annual year effects for survival.  
1440 Histograms include 7500 post-warmup MCMC samples for symbiotic (S+; blue) and symbiont-free  
1441 (S-; tan) plants from fitted vital rate model.



1457 **Fig. S12** Posterior distributions of the standard deviations of inter-annual year effects for seedling survival. Histograms include 7500 post-warmup MCMC samples for symbiotic (S+; blue) and symbiont-free (S-; tan) plants from fitted vital rate model.

1459  
1460  
1461  
1462  
1463  
1464  
1465  
1466  
1467  
1468  
1469  
1470  
1471  
1472

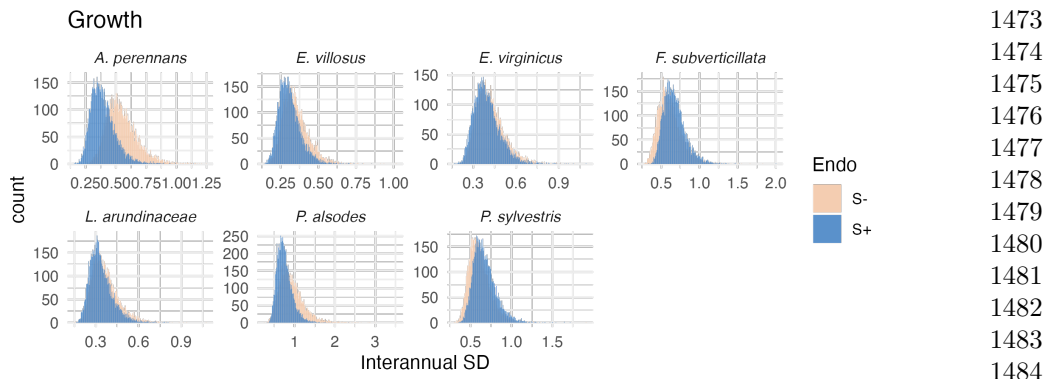


**Fig. S13** Posterior distributions of the standard deviations of inter-annual year effects for growth. Histograms include 7500 post-warmup MCMC samples for symbiotic (S+; blue) and symbiont-free (S-; tan) plants from fitted vital rate model.

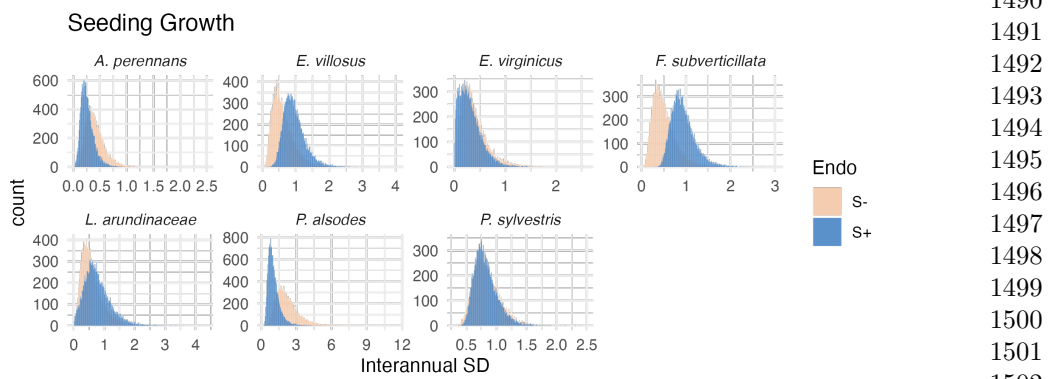
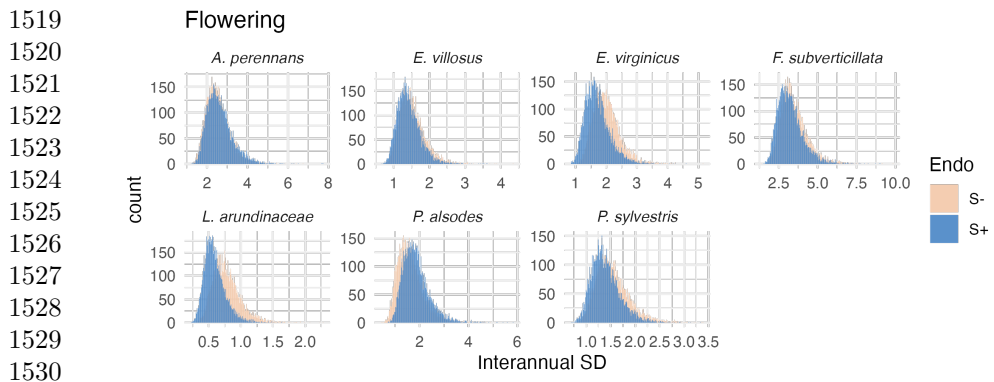
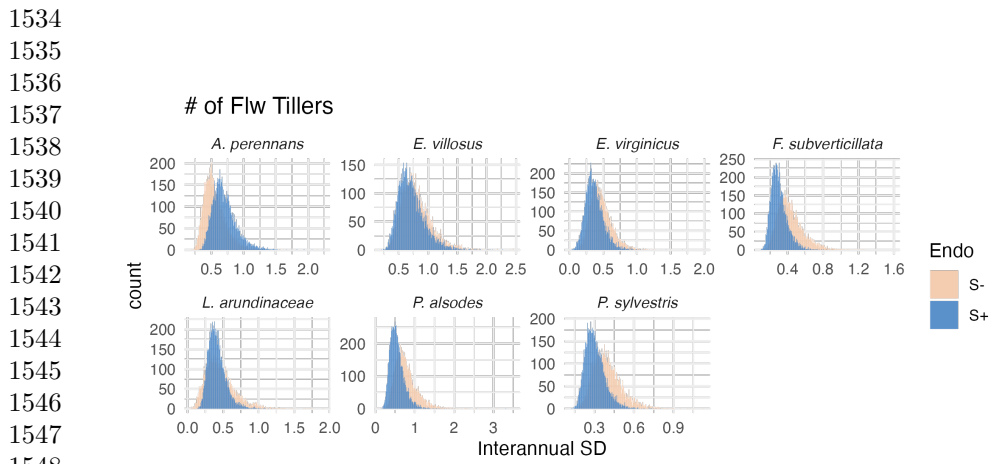


**Fig. S14** Posterior distributions of the standard deviations of inter-annual year effects for seedling growth. Histograms include 7500 post-warmup MCMC samples for symbiotic (S+; blue) and symbiont-free (S-; tan) plants from fitted vital rate model.

1473  
1474  
1475  
1476  
1477  
1478  
1479  
1480  
1481  
1482  
1483  
1484  
1485  
1486  
1487  
1488  
1489  
1490  
1491  
1492  
1493  
1494  
1495  
1496  
1497  
1498  
1499  
1500  
1501  
1502  
1503  
1504  
1505  
1506  
1507  
1508  
1509  
1510  
1511  
1512  
1513  
1514  
1515  
1516  
1517  
1518



1531 **Fig. S15** Posterior distributions of the standard deviations of inter-annual year effects for flowering  
 1532 probability. Histograms include 7500 post-warmup MCMC samples for symbiotic (S+; blue) and  
 1533 symbiont-free (S-; tan) plants from fitted vital rate model.



1549 **Fig. S16** Posterior distributions of the standard deviations of inter-annual year effects for fertility  
 1550 (no. of flowering tillers). Histograms include 7500 post-warmup MCMC samples for symbiotic (S+;  
 1551 blue) and symbiont-free (S-; tan) plants from fitted vital rate model.

1551  
 1552  
 1553  
 1554  
 1555  
 1556  
 1557  
 1558  
 1559  
 1560  
 1561  
 1562  
 1563  
 1564

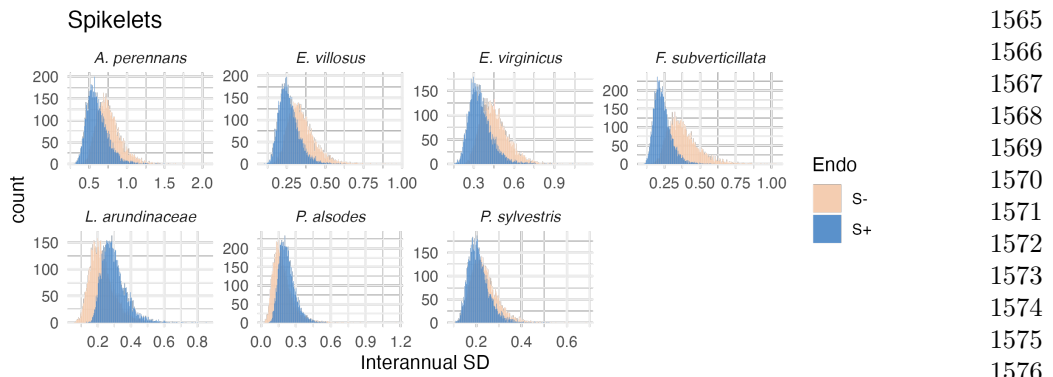


**Fig. S17** Posterior distributions of the standard deviations of inter-annual year effects for spikelets per inflorescence. Histograms include 7500 post-warmup MCMC samples for symbiotic (S+; blue) and symbiont-free (S-; tan) plants from fitted vital rate model.

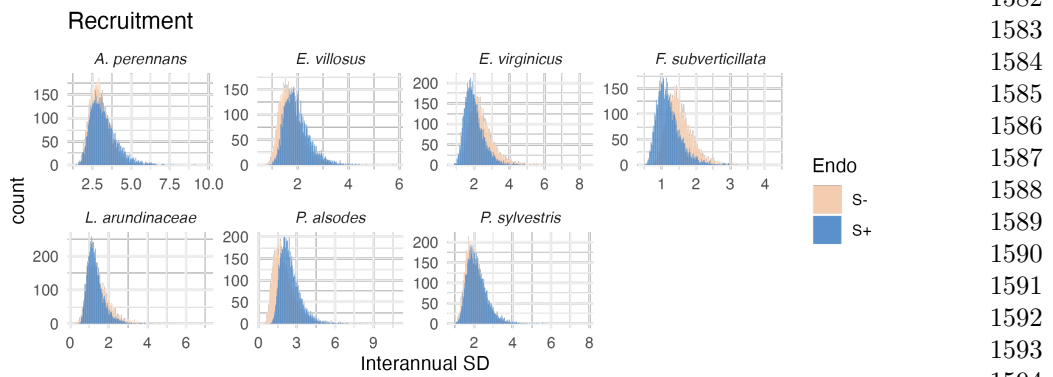
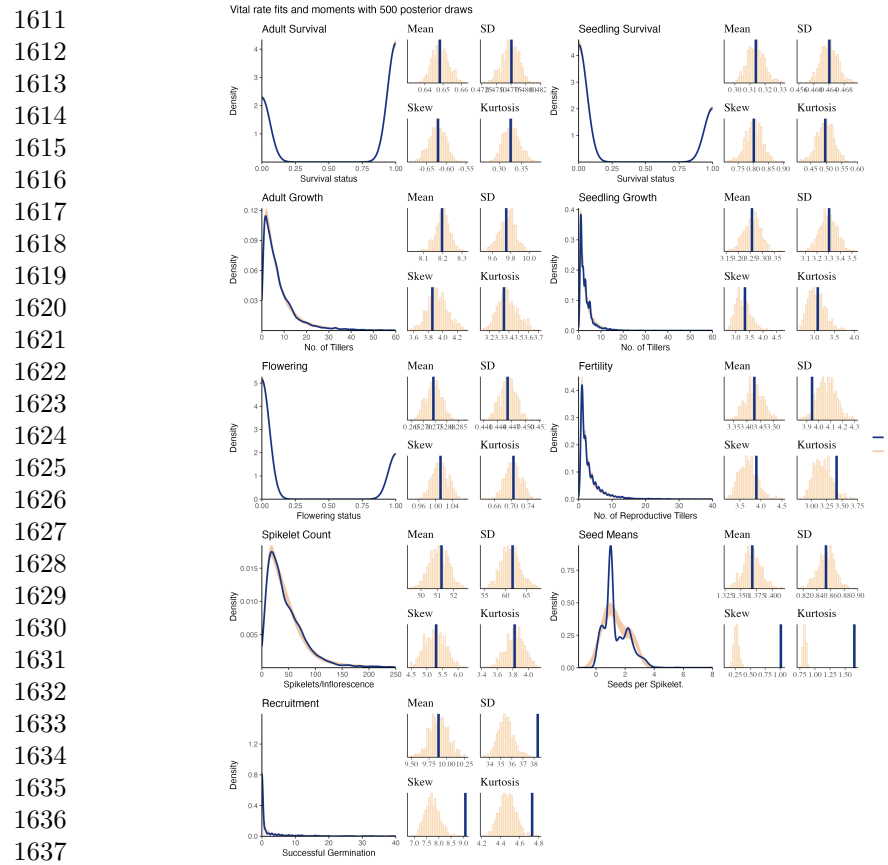


**Fig. S18** Posterior distributions of the standard deviations of inter-annual year effects for recruitment. Histograms include 7500 post-warmup MCMC samples for symbiotic (S+; blue) and symbiont-free (S-; tan) plants from fitted vital rate model.



1638 **Fig. S19** Consistency between real data and simulated values indicates that fitted models describe  
1639 the data well. Graphs show posterior predictive check for statistical models of demographic vital  
1640 rates. Lines show density distributions of observed data (blue line) compared to data simulated from  
1641 fitted models (tan lines) generated from 500 draws from posterior distributions of model parameters.

1642  
1643  
1644  
1645  
1646  
1647  
1648  
1649  
1650  
1651  
1652  
1653  
1654  
1655  
1656

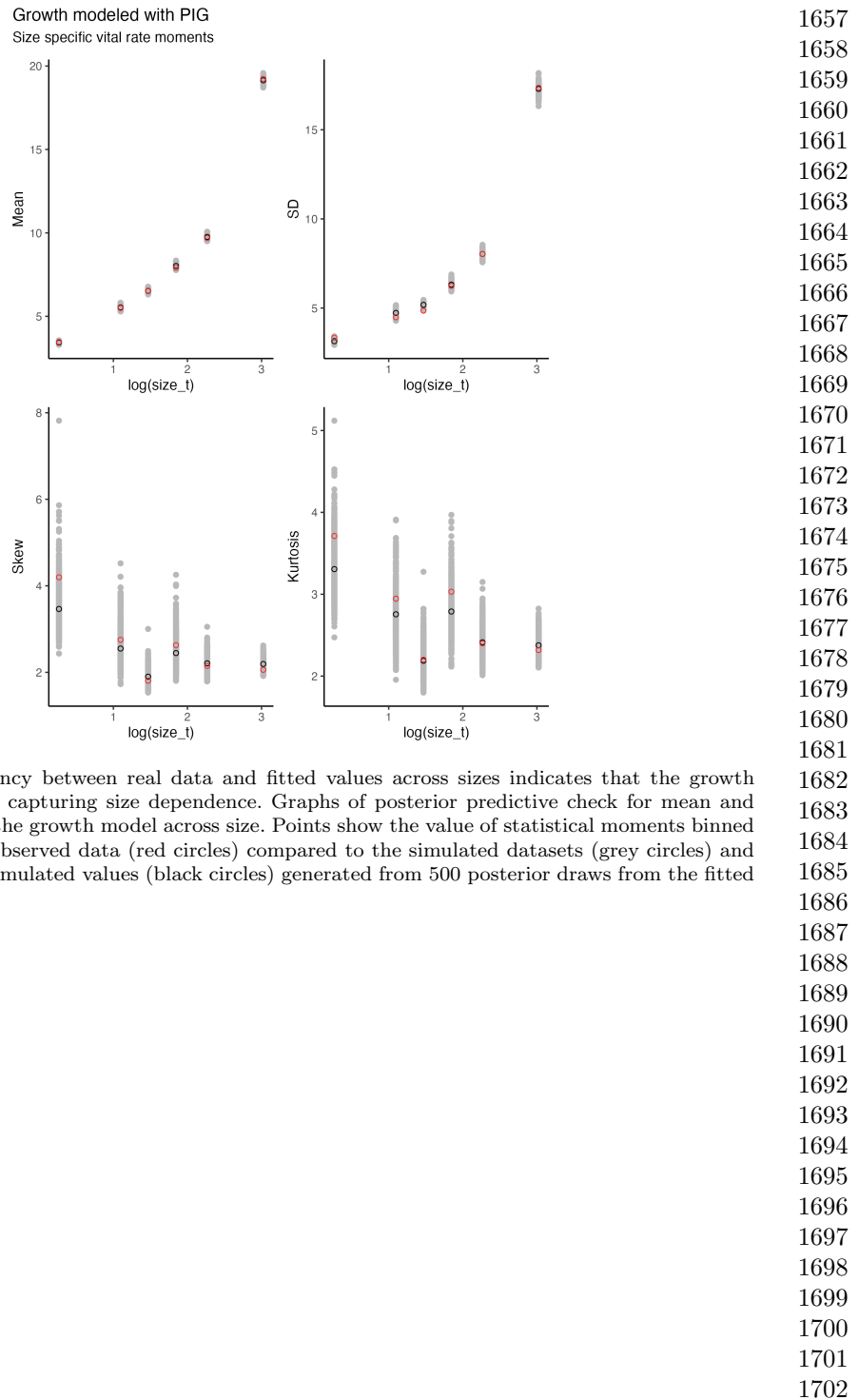
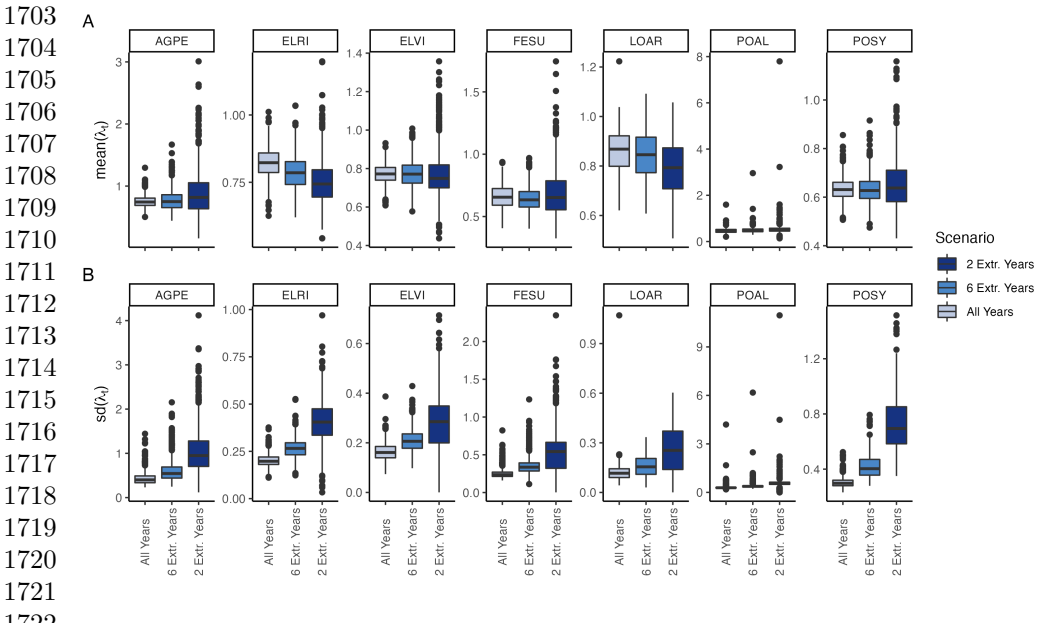
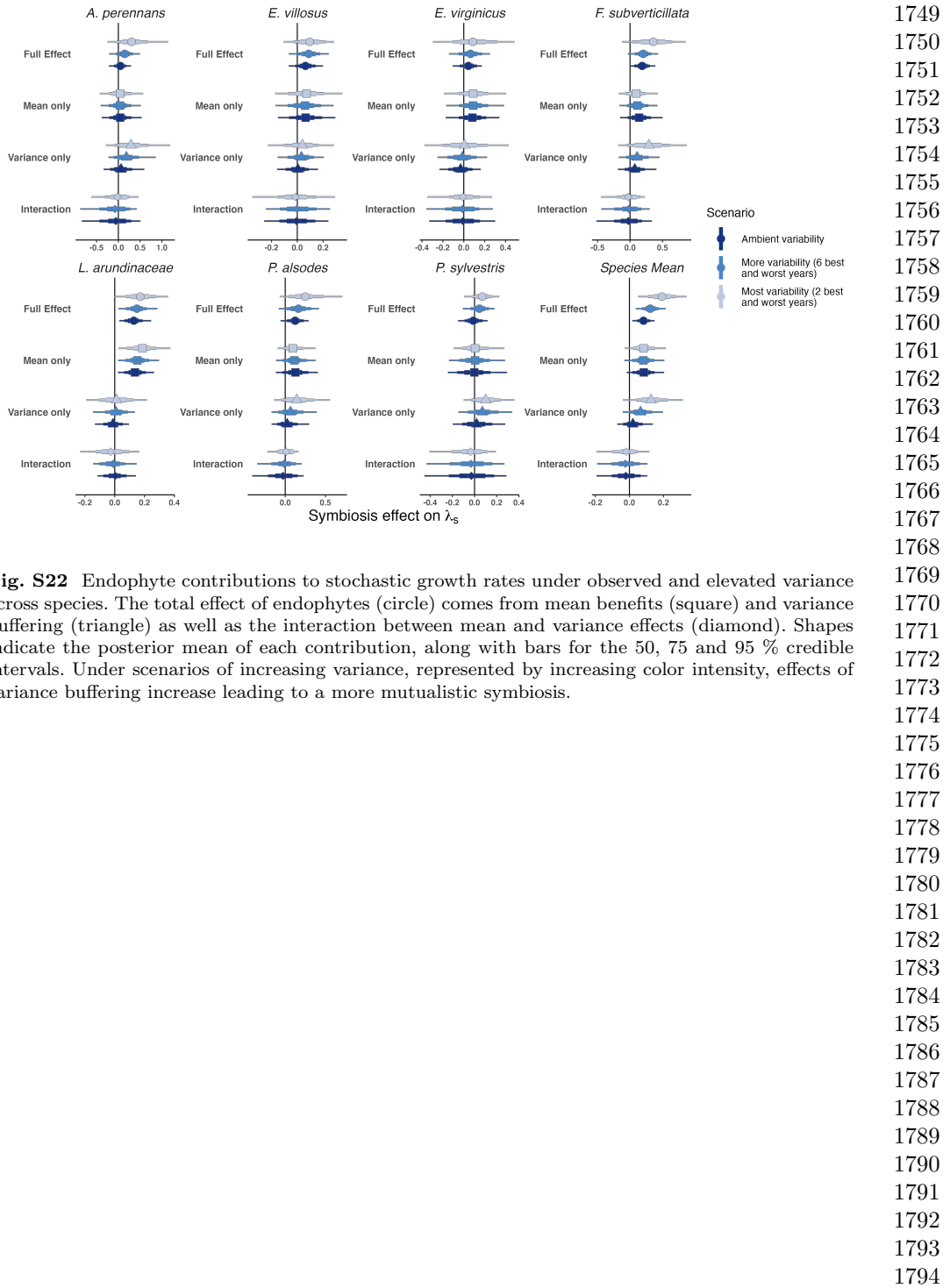


**Fig. S20** Consistency between real data and fitted values across sizes indicates that the growth model is accurately capturing size dependence. Graphs of posterior predictive check for mean and higher moments of the growth model across size. Points show the value of statistical moments binned across size for the observed data (red circles) compared to the simulated datasets (grey circles) and the median of the simulated values (black circles) generated from 500 posterior draws from the fitted model.



1723 **Fig. S21** (A) Mean and (B) standard deviation of annual growth rate values during simulation  
1724 scenarios. Each scenario selects from observed transition matrixes, increasing the variance by selecting  
1725 either all observed years, or a set (6 or 2 years) that have the highest and lowest growth rates for  
1726 symbiont-free populations.

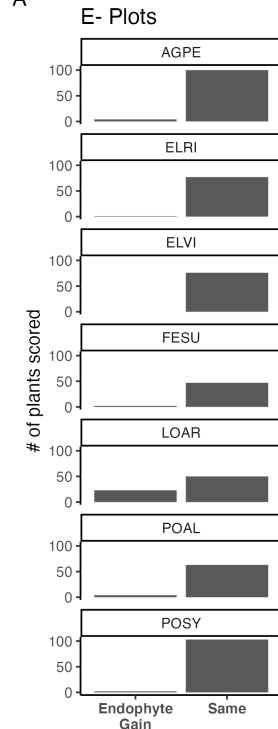
1726  
1727  
1728  
1729  
1730  
1731  
1732  
1733  
1734  
1735  
1736  
1737  
1738  
1739  
1740  
1741  
1742  
1743  
1744  
1745  
1746  
1747  
1748



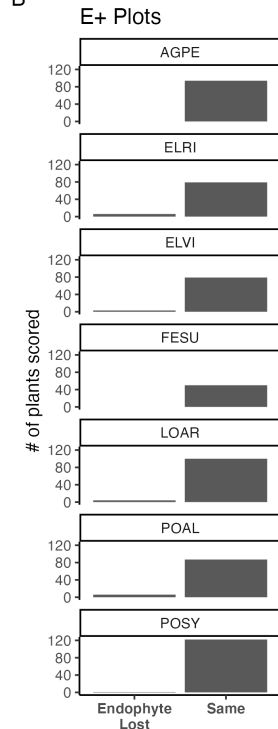
1795  
1796  
1797  
1798  
1799  
1800  
1801  
1802  
1803  
1804  
1805  
1806  
1807  
1808  
1809  
1810  
1811  
1812  
1813  
1814  
1815  
1816  
1817  
1818  
1819  
1820

#### Endophyte Status Checks

A

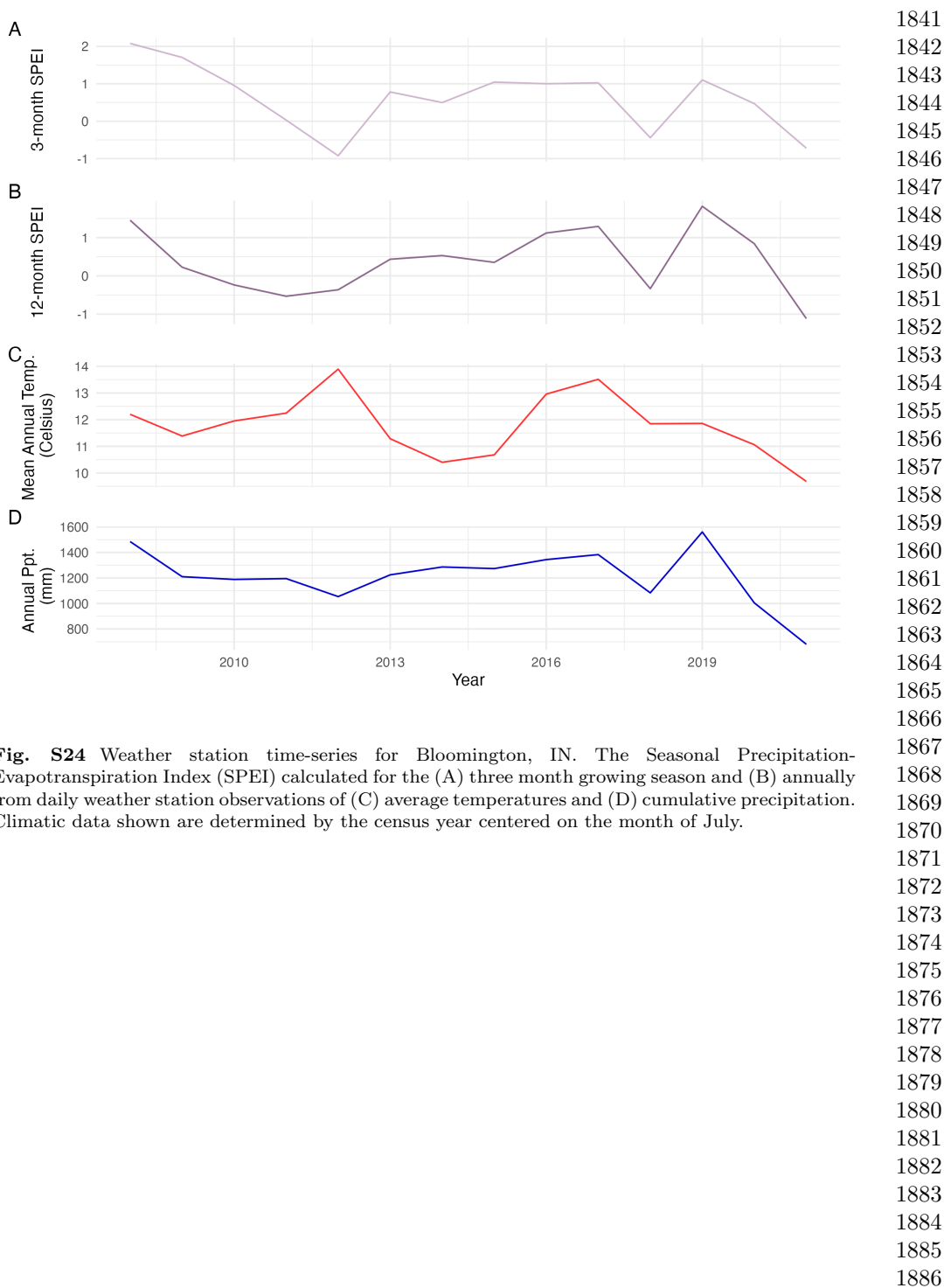


B

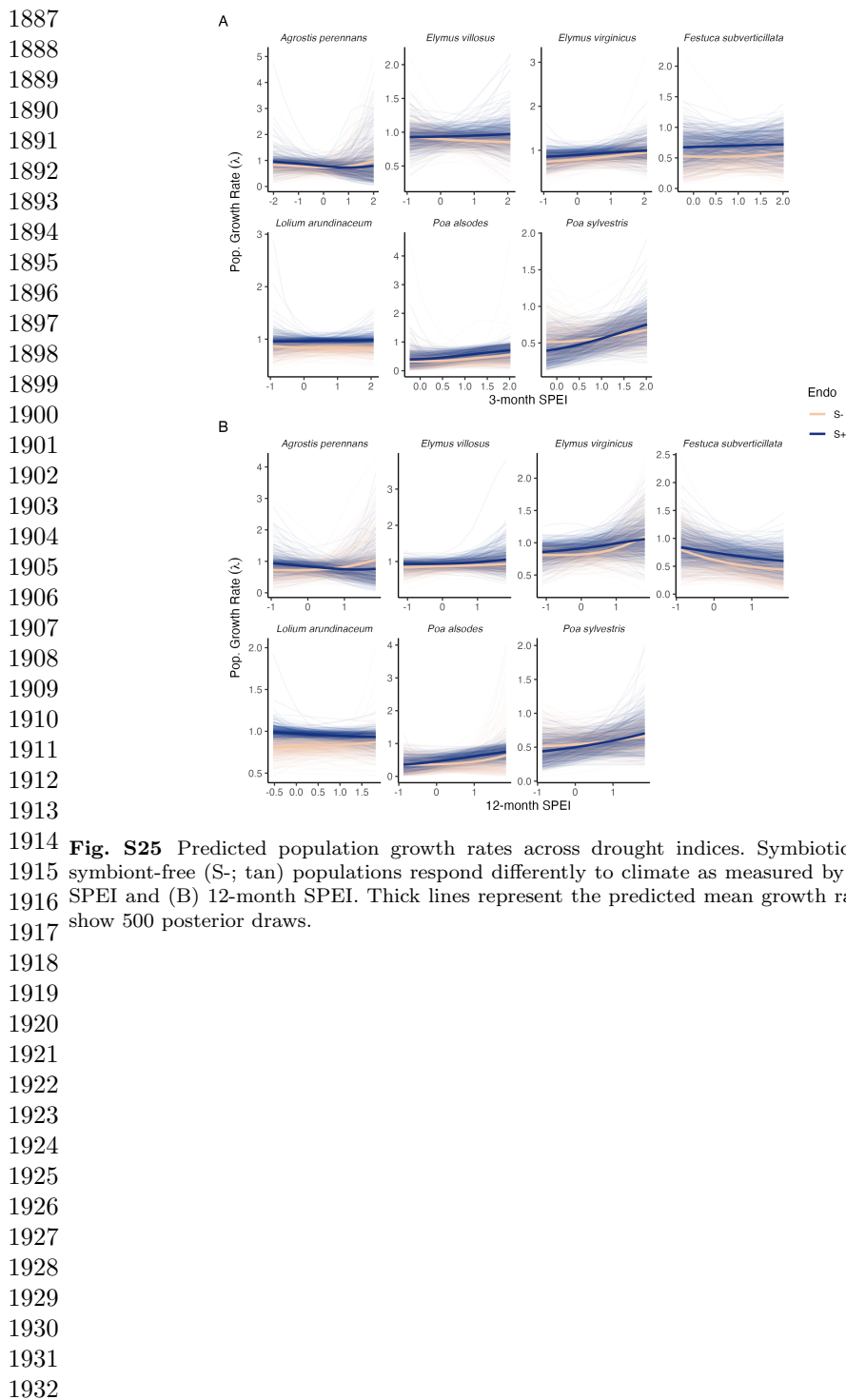


1821 **Fig. S23** Faithfulness of experimental plots to assigned endophyte status. Counts of plants scored  
1822 with leaf peels or seed squashes to check the faithfulness of recruits to the assigned plot-level endophyte  
1823 status. (A) Endophytic plants may be gained in initially S- plots, or (B) lost in initially S+ plots.

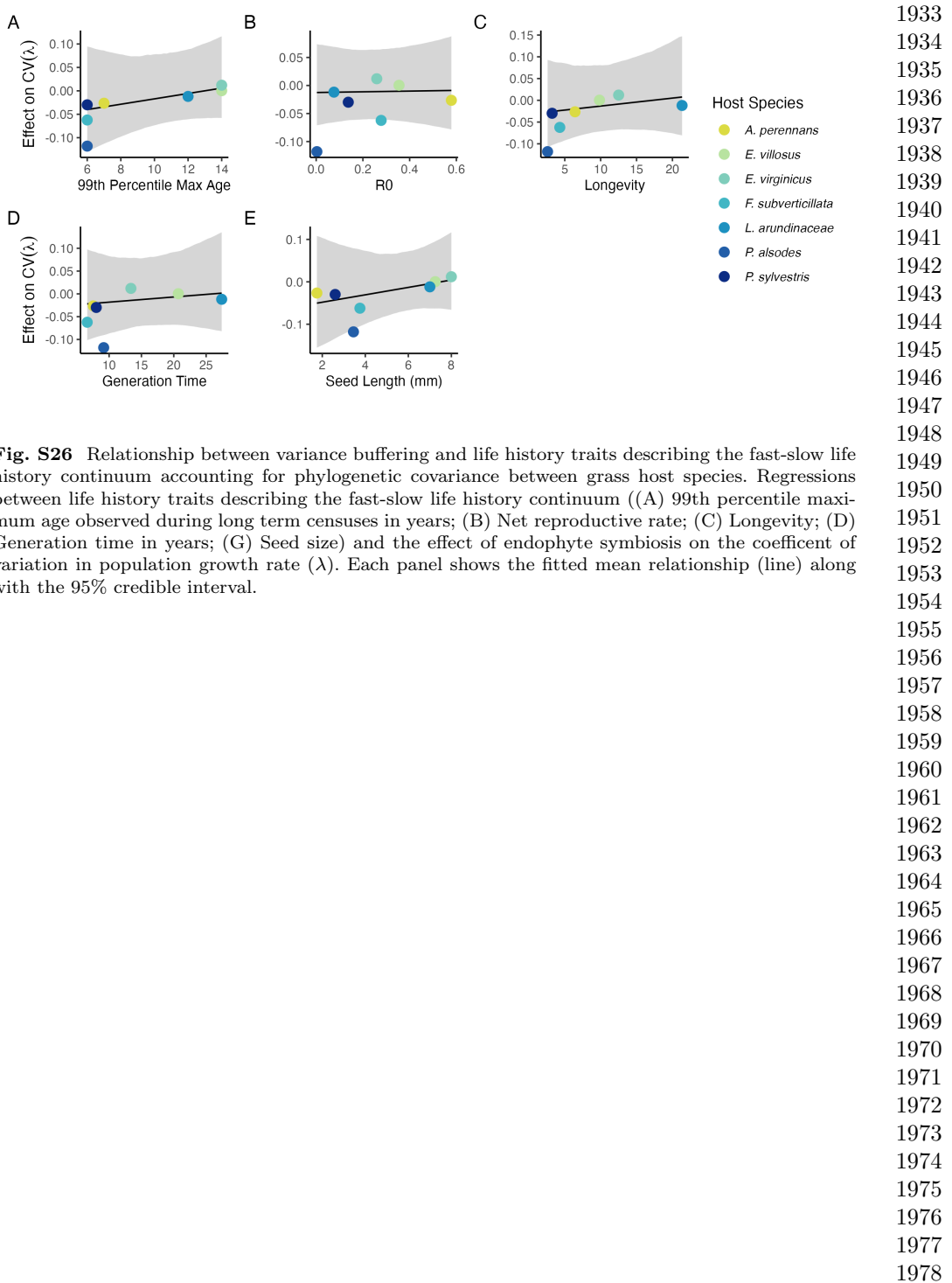
1824  
1825  
1826  
1827  
1828  
1829  
1830  
1831  
1832  
1833  
1834  
1835  
1836  
1837  
1838  
1839  
1840



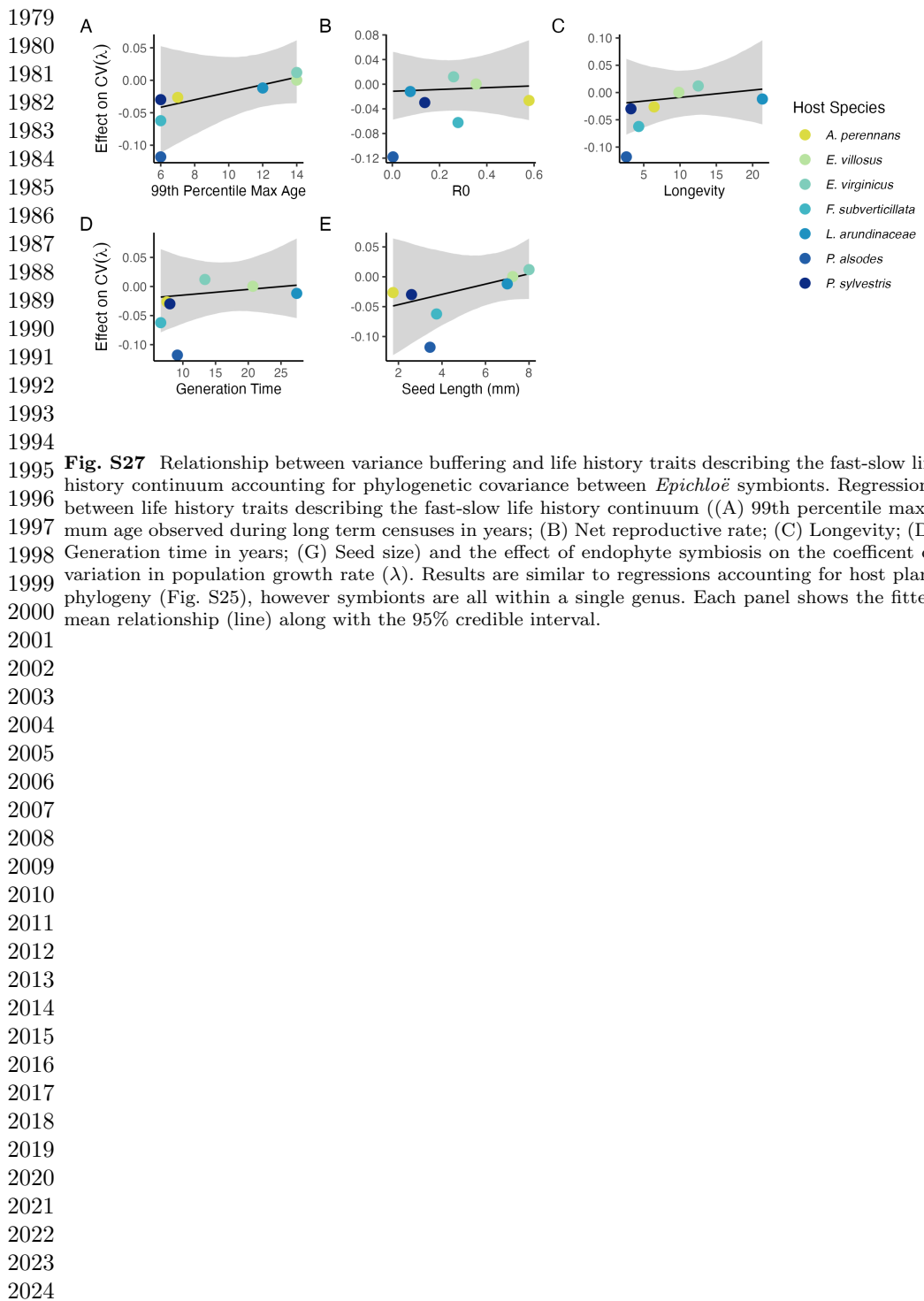
**Fig. S24** Weather station time-series for Bloomington, IN. The Seasonal Precipitation-Evapotranspiration Index (SPEI) calculated for the (A) three month growing season and (B) annually from daily weather station observations of (C) average temperatures and (D) cumulative precipitation. Climatic data shown are determined by the census year centered on the month of July.



**Fig. S25** Predicted population growth rates across drought indices. Symbiotic (S+; blue) and symbiont-free (S-; tan) populations respond differently to climate as measured by the (A) 3-month SPEI and (B) 12-month SPEI. Thick lines represent the predicted mean growth rate and thin lines show 500 posterior draws.



**Fig. S26** Relationship between variance buffering and life history traits describing the fast-slow life history continuum accounting for phylogenetic covariance between grass host species. Regressions between life history traits describing the fast-slow life history continuum ((A) 99th percentile maximum age observed during long term censuses in years; (B) Net reproductive rate; (C) Longevity; (D) Generation time in years; (E) Seed size) and the effect of endophyte symbiosis on the coefficient of variation in population growth rate ( $\lambda$ ). Each panel shows the fitted mean relationship (line) along with the 95% credible interval.



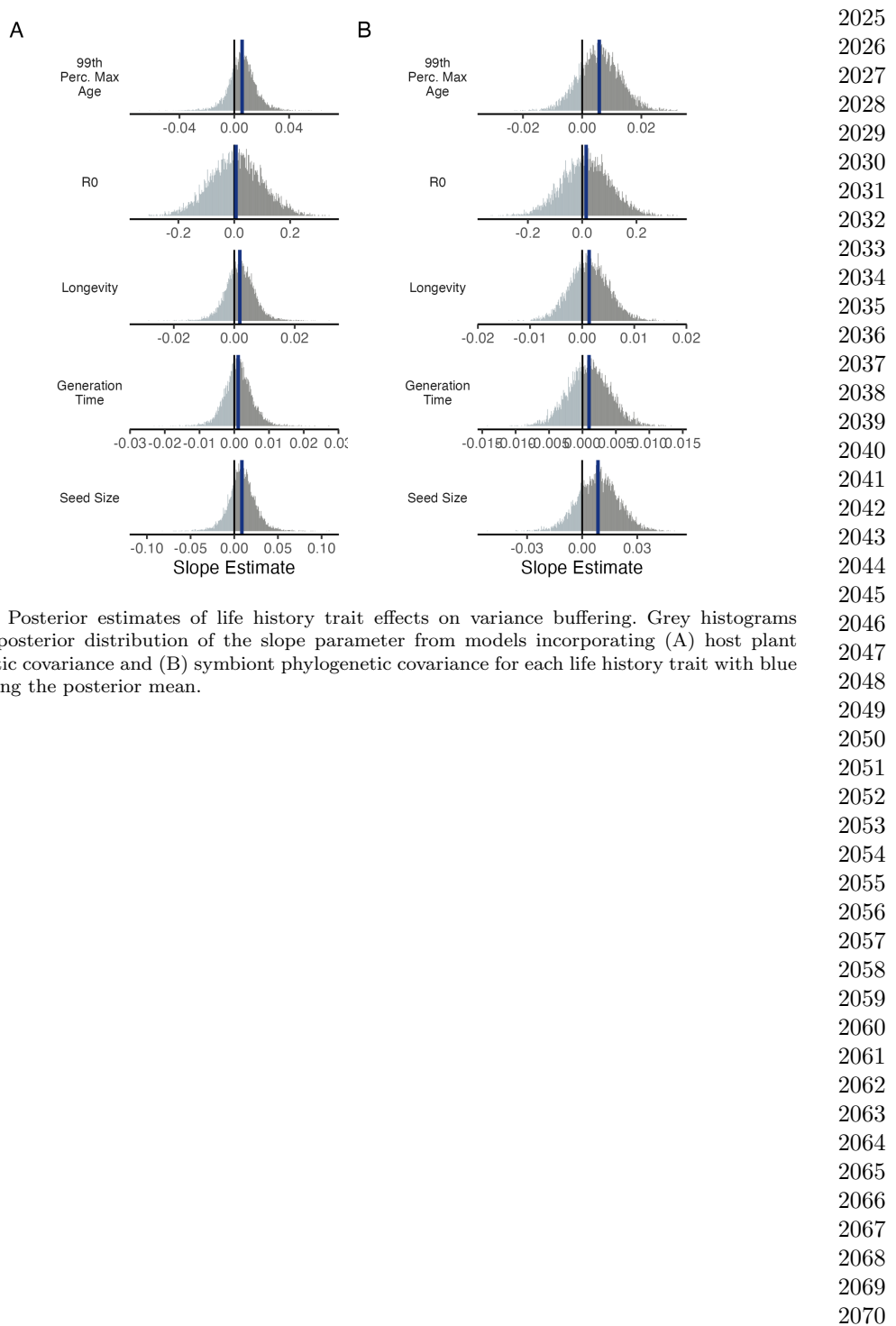


**Fig. S28** Posterior estimates of life history trait effects on variance buffering. Grey histograms show the posterior distribution of the slope parameter from models incorporating (A) host plant phylogenetic covariance and (B) symbiont phylogenetic covariance for each life history trait with blue bars showing the posterior mean.

2071 **Supplemental Tables S1-S3**

2072

2073

2074

2075

2076

2077

2078

2079

2080

2081

2082

2083

2084

2085

2086

2087

2088

2089

2090

2091

2092

2093

2094

2095

2096

2097

2098

2099

2100

2101

2102

2103

2104

2105

2106

2107

2108

2109

2110

2111

2112

2113

2114

2115

2116

**Table S1** Summary of host-endophyte propagation and transplant methods

Host Species	Symbiont Species	Heat treatment duration (Temp.)	Transplant date
<i>Agrostis perennans</i>	<i>E. amarillans</i>	12 min. hot water bath (60 °C)	April 2008 (10 plots)
<i>Elymus villosus</i>	<i>E. elymi</i>	6 days drying oven (60 °C)	April 2008 (10 plots)
<i>Elymus virginicus</i>	<i>E. elymi</i> or <i>EviTG-1</i>	6 days drying oven (60 °C)	April 2008 (10 plots)
<i>Festuca subverticillata</i>	<i>E. starrii</i>	6 days drying oven (60 °C)	April 2008 (10 plots)
<i>Lolium arundinaceum</i>	<i>E. coenophiala</i>	6 days drying oven (60 °C)	Sept. 2007 (10 plots)
<i>Poa alsodes</i>	<i>E. alsodes</i>	7 days drying oven (60 °C)	Sept. 2007 (8 plots)/April 2008 (10 plots)
<i>Poa sylvestris</i>	<i>E. PsyTG-1</i>	7 days drying oven (60 °C)	Sept. 2007 (8 plots)/April 2008 (10 plots)
			2117
			2118
			2119
			2120
			2121
			2122
			2123
			2124
			2125
			2126
			2127
			2128
			2129
			2130
			2131
			2132
			2133
			2134
			2135
			2136
			2137
			2138
			2139
			2140
			2141
			2142
			2143
			2144
			2145
			2146
			2147
			2148
			2149
			2150
			2151
			2152
			2153
			2154
			2155
			2156
			2157
			2158
			2159
			2160
			2161
			2162

2163  
 2164  
 2165  
 2166  
 2167  
 2168  
 2169  
 2170  
 2171  
 2172  
 2173  
 2174  
 2175  
 2176  
 2177  
 2178  
 2179  
 2180  
 2181  
 2182  
 2183  
 2184  
 2185  
 2186  
 2187  
 2188  
 2189  
 2190  
 2191  
 2192  
 2193  
 2194  
 2195  
 2196  
 2197  
 2198  
 2199  
 2200  
 2201  
 2202  
 2203  
 2204  
 2205  
 2206  
 2207  
 2208

**Table S2** Summary of focal life history traits

Host Species	Observed max age (years)	99th percentile max age (years)	Generation time (years)	$R_0$	Longevity (years)	Seed length (mm.)	Imperfect transmission rate (%)	Stromata Observed of indiv. per species)
<i>Agrostis perennans</i>	11	7	7.6	0.58	6.4	1.75	69.8	0.0
<i>Elymus villosus</i>	14	14	20.7	0.35	9.8	7.25	100	4.6
<i>Elymus virginicus</i>	14	14	13.4	0.25	12.5	8	100	0.6
<i>Festuca subverticillata</i>	9	6	6.6	0.28	4.3	3.75	42.7	0.0
<i>Lolium arundinaceum</i>	12*	12*	27.4	0.08	21.3	7	100	0.0
<i>Poa alsodes</i>	8	6	9.2	0.003	2.6	3.45	99.9	0.0
<i>Poa syriaca</i>	12	6	8.0	0.14	3.2	2.6	16.6	0.1

\*Censuses for *L. arundinaceum* plots stopped after year 12 of the experiment.

**Table S3** Summary of host-endophyte drought sensitivities

Host Species	Effect on CV( $\lambda$ )	Effect on Mean( $\lambda$ )	$\frac{\Delta\lambda^-}{\Delta SPEI_3}$	$\frac{\Delta\lambda^+}{\Delta SPEI_3}$	3 month S- to S+ ratio	$\frac{\Delta\lambda^-}{\Delta SPEI_{12}}$	$\frac{\Delta\lambda^+}{\Delta SPEI_{12}}$	12 month S- to S+ ratio
<i>Agrostis perennans</i>	-0.0264	0.0441	0.03	-0.04	0.85	0.11	-0.06	1.82
<i>Elymus villosus</i>	0.0003	0.0509	-0.03	0.01	1.95	0.03	0.04	0.70
<i>Elymus virginicus</i>	0.0120	0.0578	0.07	0.05	1.50	0.10	0.07	1.42
<i>Festuca subverticillata</i>	-0.0622	0.1639	0.02	0.02	1.01	-0.13	-0.09	1.43
<i>Lolium arundinaceum</i>	-0.0118	0.1022	-0.01	0.01	1.32	0.03	-0.03	1.02
<i>Poa alsodes</i>	-0.1179	0.1282	0.10	0.14	0.71	0.11	0.14	0.73
<i>Poa sylvestris</i>	-0.0298	-0.0085	0.07	0.16	0.44	0.05	0.10	0.55
								2209
								2210
								2211
								2212
								2213
								2214
								2215
								2216
								2217
								2218
								2219
								2220
								2221
								2222
								2223
								2224
								2225
								2226
								2227
								2228
								2229
								2230
								2231
								2232
								2233
								2234
								2235
								2236
								2237
								2238
								2239
								2240
								2241
								2242
								2243
								2244
								2245
								2246
								2247
								2248
								2249
								2250
								2251
								2252
								2253
								2254

2255 **References**

- 2256  
2257 [1] Seneviratne, S. *et al.* *Changes in climate extremes and their impacts on the*  
2258 *natural physical environment* (Cambridge University Press, 2012).
- 2259  
2260 [2] IPCC. Climate change 2021: The physical science basis (2021). URL <https://www.ipcc.ch/report/ar6/wg1/>.
- 2261  
2262 [3] Lewontin, R. C. & Cohen, D. On Population Growth in a Randomly Varying Envi-  
2263 ronment. *Proceedings of the National Academy of Sciences* **62**, 1056–1060 (1969).  
2264 URL <https://www.pnas.org/content/62/4/1056>. Publisher: National Academy of  
2265 Sciences Section: Biological Sciences: Zoology.
- 2266  
2267 [4] Tuljapurkar, S. D. Population dynamics in variable environments. III. Evolution-  
2268 ary dynamics of r-selection. *Theoretical Population Biology* **21**, 141–165 (1982).  
2269 URL <http://www.sciencedirect.com/science/article/pii/0040580982900107>.
- 2270  
2271 [5] Cohen, J. E. Comparative statics and stochastic dynamics of age-structured  
2272 populations. *Theoretical population biology* **16**, 159–171 (1979).
- 2273  
2274 [6] Tuljapurkar, S. *Population dynamics in variable environments* Vol. 85 (Springer  
2275 Science & Business Media, 2013).
- 2276  
2277 [7] Pfister, C. A. Patterns of variance in stage-structured populations: evolutionary  
2278 predictions and ecological implications. *Proceedings of the National Academy of  
2279 Sciences* **95**, 213–218 (1998).
- 2280  
2281 [8] Morris, W. F. *et al.* Longevity can buffer plant and animal populations against  
2282 changing climatic variability. *Ecology* **89**, 19–25 (2008).
- 2283  
2284 [9] Compagnoni, A. *et al.* The effect of demographic correlations on the stochastic  
2285 population dynamics of perennial plants. *Ecological Monographs* **86**, 480–494  
2286 (2016).
- 2287  
2288 [10] Ellis, M. M. & Crone, E. E. The role of transient dynamics in stochastic  
2289 population growth for nine perennial plants. *Ecology* **94**, 1681–1686 (2013).
- 2290  
2291 [11] Rodríguez-Caro, R. C. *et al.* The limits of demographic buffering in coping with  
2292 environmental variation. *Oikos* **130**, 1346–1358 (2021).
- 2293  
2294 [12] Tuljapurkar, S. & Orzack, S. H. Population dynamics in variable environments i.  
2295 long-run growth rates and extinction. *Theoretical Population Biology* **18**, 314–342  
2296 (1980).
- 2297  
2298 [13] Fieberg, J. & Ellner, S. P. Stochastic matrix models for conservation and  
2299 management: a comparative review of methods. *Ecology letters* **4**, 244–266 (2001).
- 2300

- [14] Menges, E. S. Applications of population viability analyses in plant conservation. *Ecological Bulletins* 73–84 (2000). 2301  
2302  
2303
- [15] Kuparinen, A., Boit, A., Valdovinos, F. S., Lassaux, H. & Martinez, N. D. Fishing-induced life-history changes degrade and destabilize harvested ecosystems. *Scientific reports* **6**, 22245 (2016). 2304  
2305  
2306  
2307
- [16] Hilde, C. H. *et al.* The Demographic Buffering Hypothesis: Evidence and Challenges. *Trends in Ecology & Evolution* **0** (2020). URL [https://www.cell.com/trends/ecology-evolution/abstract/S0169-5347\(20\)30050-1](https://www.cell.com/trends/ecology-evolution/abstract/S0169-5347(20)30050-1). Publisher: Elsevier. 2308  
2309  
2310  
2311
- [17] Rodriguez, R., White Jr, J., Arnold, A. E. & Redman, a. R. a. Fungal endophytes: diversity and functional roles. *New phytologist* **182**, 314–330 (2009). 2312  
2313
- [18] McFall-Ngai, M. *et al.* Animals in a bacterial world, a new imperative for the life sciences. *Proceedings of the National Academy of Sciences* **110**, 3229–3236 (2013). 2314  
2315  
2316  
2317
- [19] Funkhouser, L. J. & Bordenstein, S. R. Mom knows best: the universality of maternal microbial transmission. *PLoS biology* **11**, e1001631 (2013). 2318  
2319  
2320
- [20] Fine, P. E. Vectors and vertical transmission: an epidemiologic perspective. *Annals of the New York Academy of Sciences* **266**, 173–194 (1975). 2321  
2322  
2323
- [21] Russell, J. A. & Moran, N. A. Costs and benefits of symbiont infection in aphids: variation among symbionts and across temperatures. *Proceedings of the Royal Society B: Biological Sciences* **273**, 603–610 (2006). 2324  
2325  
2326  
2327
- [22] Kivlin, S. N., Emery, S. M. & Rudgers, J. A. Fungal symbionts alter plant responses to global change. *American Journal of Botany* **100**, 1445–1457 (2013). 2328  
2329
- [23] Dunbar, H. E., Wilson, A. C. C., Ferguson, N. R. & Moran, N. A. Aphid thermal tolerance is governed by a point mutation in bacterial symbionts. *PLoS biology* **5**, e96 (2007). 2330  
2331  
2332  
2333
- [24] Reyna, R., Cooke, P., Grum, D., Cook, D. & Creamer, R. Detection and localization of the endophyte undifilum oxytropis in locoweed tissues. *Botany* **90**, 1229–1236 (2012). 2334  
2335  
2336  
2337
- [25] Saikkinen, K., Gundel, P. E. & Helander, M. Chemical ecology mediated by fungal endophytes in grasses. *Journal of chemical ecology* **39**, 962–968 (2013). 2338  
2339  
2340
- [26] Neyaz, M., Gardner, D. R., Creamer, R. & Cook, D. Localization of the swainsonine-producing chaetothyriales symbiont in the seed and shoot apical meristem in its host ipomoea carnea. *Microorganisms* **10**, 545 (2022). 2341  
2342  
2343  
2344
- [27] Chamberlain, S. A., Bronstein, J. L. & Rudgers, J. A. How context dependent are species interactions? *Ecology letters* **17**, 881–890 (2014). 2345  
2346

- 2347 [28] Jordano, P. Spatial and temporal variation in the avian-frugivore assemblage of  
2348 prunus mahaleb: patterns and consequences. *Oikos* **479–491** (1994).
- 2349
- 2350 [29] Leuchtmann, A. Systematics, distribution, and host specificity of grass endo-  
2351 phytes. *Natural toxins* **1**, 150–162 (1992).
- 2352
- 2353 [30] Cheplick, G. P., Faeth, S. & Faeth, S. H. *Ecology and evolution of the grass-*  
2354 *endophyte symbiosis* (OUP USA, 2009).
- 2355
- 2356 [31] Brem, D. & Leuchtmann, A. Epichloë grass endophytes increase herbivore resis-  
2357 tance in the woodland grass *brachypodium sylvaticum*. *Oecologia* **126**, 522–530  
2358 (2001).
- 2359
- 2360 [32] Decunta, F. A., Pérez, L. I., Malinowski, D. P., Molina-Montenegro, M. A. &  
2361 Gundel, P. E. A systematic review on the effects of epichloë fungal endophytes  
2362 on drought tolerance in cool-season grasses. *Frontiers in plant science* **12**, 644731  
2363 (2021).
- 2364
- 2365 [33] Bacon, C. W. & White, J. F. in *Stains, media, and procedures for analyzing*  
2366 *endophytes* 47–56 (CRC Press, 2018).
- 2367
- 2368 [34] Rudgers, J. A. & Swafford, A. L. Benefits of a fungal endophyte in *elymus*  
2369 *virginicus* decline under drought stress. *Basic and Applied Ecology* **10**, 43–51  
2370 (2009).
- 2371
- 2372 [35] Bultman, T. L., White Jr, J. F., Bowdish, T. I., Welch, A. M. & Johnston, J.  
2373 Mutualistic transfer of epichloë spermatia by phorbia flies. *Mycologia* **87**, 182–189  
2374 (1995).
- 2375
- 2376 [36] Stan Development Team. RStan: the R interface to Stan (2022). URL <https://mc-stan.org/>. R package version 2.21.7.
- 2377
- 2378 [37] Elderd, B. D. & Miller, T. E. Quantifying demographic uncertainty: Bayesian  
2379 methods for integral projection models. *Ecological Monographs* **86**, 125–144  
2380 (2016).
- 2381
- 2382 [38] Gabry, J., Simpson, D., Vehtari, A., Betancourt, M. & Gelman, A. Visualization  
2383 in bayesian workflow. *Journal of the Royal Statistical Society Series A: Statistics*  
2384 in Society **182**, 389–402 (2019).
- 2385
- 2386 [39] Brooks, S. P. & Gelman, A. General methods for monitoring convergence of  
2387 iterative simulations. *Journal of computational and graphical statistics* **7**, 434–455  
2388 (1998).
- 2389
- 2390 [40] Gelman, A. & Hill, J. *Data analysis using regression and multilevel/hierarchical*  
2391 *models* (Cambridge university press, 2006).
- 2392

- [41] Williams, J. L., Miller, T. E. & Ellner, S. P. Avoiding unintentional eviction from integral projection models. *Ecology* **93**, 2008–2014 (2012). 2393  
2394  
2395
- [42] Jones, O. R. *et al.* Rcompadre and rage—two r packages to facilitate the use of the compadre and comadre databases and calculation of life-history traits from matrix population models. *Methods in Ecology and Evolution* **13**, 770–781 (2022). 2396  
2397  
2398
- [43] . 2399  
2400
- [44] Bürkner, P.-C. brms: An R package for Bayesian multilevel models using Stan. *Journal of Statistical Software* **80**, 1–28 (2017). 2401  
2402  
2403
- [45] Zanne, A. E. *et al.* Three keys to the radiation of angiosperms into freezing environments. *Nature* **506**, 89–92 (2014). 2404  
2405  
2406
- [46] Leuchtmann, A., Bacon, C. W., Schardl, C. L., White Jr, J. F. & Tadych, M. Nomenclatural realignment of neotyphodium species with genus epichloë. *Mycologia* **106**, 202–215 (2014). 2407  
2408  
2409
- [47] Metcalf, C. J. E. *et al.* Statistical modelling of annual variation for inference on stochastic population dynamics using integral projection models. *Methods in Ecology and Evolution* **6**, 1007–1017 (2015). 2410  
2411  
2412  
2413
- [48] Caswell, H. Matrix population models: Construction, analysis, and interpretation. 2nd edn sinauer associates. Inc., Sunderland, MA (2001). 2414  
2415  
2416
- [49] Rees, M. & Ellner, S. P. Integral projection models for populations in temporally varying environments. *Ecological Monographs* **79**, 575–594 (2009). 2417  
2418  
2419
- [50] Vicente-Serrano, S. M., Beguería, S. & López-Moreno, J. I. A multiscalar drought index sensitive to global warming: the standardized precipitation evapotranspiration index. *Journal of climate* **23**, 1696–1718 (2010). 2420  
2421  
2422  
2423
- [51] Rudgers, J. A. & Clay, K. An invasive plant–fungal mutualism reduces arthropod diversity. *Ecology Letters* **11**, 831–840 (2008). 2424  
2425  
2426
- [52] Crawford, K. M., Land, J. M. & Rudgers, J. A. Fungal endophytes of native grasses decrease insect herbivore preference and performance. *Oecologia* **164**, 431–444 (2010). 2427  
2428  
2429  
2430
- [53] Murphy, G. I. Pattern in life history and the environment. *The American Naturalist* **102**, 391–403 (1968). 2431  
2432  
2433
- [54] Compagnoni, A. *et al.* Herbaceous perennial plants with short generation time have stronger responses to climate anomalies than those with longer generation time. *Nature communications* **12**, 1–8 (2021). 2434  
2435  
2436  
2437  
2438

- 2439 [55] Le Coeur, C., Yoccoz, N. G., Salguero-Gómez, R. & Vindenes, Y. Life his-  
2440 tory adaptations to fluctuating environments: Combined effects of demographic  
2441 buffering and lability. *Ecology Letters* **25**, 2107–2119 (2022).
- 2442
- 2443 [56] Rees, M. Evolutionary ecology of seed dormancy and seed size. *Philosophical  
2444 Transactions of the Royal Society of London. Series B: Biological Sciences* **351**,  
2445 1299–1308 (1996).
- 2446
- 2447 [57] Moles, A. T. & Westoby, M. Seedling survival and seed size: a synthesis of the  
2448 literature. *Journal of Ecology* **92**, 372–383 (2004).
- 2449
- 2450 [58] Afkhami, M. E. & Rudgers, J. A. Symbiosis lost: imperfect vertical transmission  
2451 of fungal endophytes in grasses. *The American Naturalist* **172**, 405–416 (2008).
- 2452
- 2453 [59] Jeschke, J. M. & Kokko, H. The roles of body size and phylogeny in fast and  
2454 slow life histories. *Evolutionary Ecology* **23**, 867–878 (2009).
- 2455
- 2456 [60] Afkhami, M. E. & Strauss, S. Y. Native fungal endophytes suppress an exotic  
2457 dominant and increase plant diversity over small and large spatial scales. *Ecology*  
2458 **97**, 1159–1169 (2016).
- 2459
- 2460 [61] Smith, E., Vaughan, G., Ketchum, R., McParland, D. & Burt, J. Symbiont  
2461 community stability through severe coral bleaching in a thermally extreme lagoon.  
2462 *Scientific Reports* **7**, 2428 (2017).
- 2463
- 2464 [62] Dallas, J. W. & Warne, R. W. Captivity and animal microbiomes: potential roles  
2465 of microbiota for influencing animal conservation. *Microbial Ecology* 1–19 (2022).
- 2466
- 2467 [63] Wu, L. *et al.* Reduction of microbial diversity in grassland soil is driven by  
2468 long-term climate warming. *Nature Microbiology* **7**, 1054–1062 (2022).
- 2469
- 2470 [64] Ehrlén, J. & Morris, W. F. Predicting changes in the distribution and abundance  
2471 of species under environmental change. *Ecology letters* **18**, 303–314 (2015).
- 2472
- 2473 [65] Chamberlain, S., Hocking, D. & Anderson, B. Package ‘rnoaa’ (2022).
- 2474
- 2475
- 2476
- 2477
- 2478
- 2479
- 2480
- 2481
- 2482
- 2483
- 2484